

Transtensional Tectonics of the Minto Flats Fault Zone and Nenana Basin, Central Alaska

by Carl Tape,^{*} Vipul Silwal,^{*} Chen Ji, Laura Keyson,^{*} Michael E. West,[†] and Natalia Ruppert[†]

Abstract Central Alaska is a broad zone of crustal deformation that is produced by collision and flat slab subduction. Within central Alaska, there are large-scale right-lateral strike-slip faults, such as the Denali fault (2002 M_w 7.9), as well as smaller-scale fold-and-thrust belts and a set of left-lateral strike-slip fault zones, one of which is the Minto Flats fault zone (MFFZ). We use seismological evidence to document a pair of overlapping left-lateral faults that define the MFFZ. Microseismicity delineates this 180-km-long fault zone. Using body waves and surface waves, we perform moment tensor inversions for the 11 best-recorded earthquakes in the fault zone. Moment tensors reveal consistent left-lateral faulting throughout the fault zone. A finite-source model for the 1995 M_w 6.0 earthquake is consistent with left-lateral faulting and provides rupture details for the largest known event in the fault zone. The two main faults are separated by 10 km and overlap by 67 km, forming a releasing stepover geometry within a local transtensional setting. Between the faults is a 90-km-long, 12-km-wide, and 8-km-deep sedimentary basin (the Nenana basin). We interpret the transtensional faulting to be responsible for the development of the basin over the past 6 Ma. The distances of fault overlap and fault separation are key parameters for determining (1) the 3D morphology of the sedimentary basin and (2) the likelihood of earthquake ruptures jumping from one fault to the next. The structure of the Nenana basin is consistent with shear motion accommodated by the identified faults. The 10 km fault separation suggests that ruptures are not likely to span the entire fault zone. Earthquakes as large as M_w 7.0–7.5 could occur on the faults. The transtensional fault zone provides an important constraint for understanding the larger-scale intraplate tectonic setting of central Alaska.

Online Material: Figures of waveform fits, depth estimation for moment tensors, variation in seismicity, and fault-plane identification.

Introduction

Central Alaska is a broad zone of intraplate tectonics manifested by seismicity, Global Positioning System (GPS) measurements, and active faults (Ruppert *et al.*, 2008). Physiographically, the region spans from the Alaska Range to the Brooks Range and includes the Yukon–Tanana uplands as well as drainage basins for the Yukon, Tanana, and Nenana Rivers (Figs. 1 and 2). Tectonically the region is partly underlain by the Pacific–Yukutat slab (Fig. 2), and it contains two major right-lateral faults: the Denali fault to the south, which produced the 2002 M_w 7.9 earthquake, and the Tintina–Kaltag fault to the north. Between these two faults are two sets of

faults that produced three $M > 7$ earthquakes in 1904, 1937, and 1947: (1) a fold-and-thrust belt near the Alaska Range (Bemis and Wallace, 2007) and (2) a series of northeast-striking seismic lineaments near the greater Fairbanks area (Page *et al.*, 1995) (Fig. S1, available in the electronic supplement to this article).

Several subparallel, northeast-striking seismic zones are visible in the greater Fairbanks area. These have been categorized into three seismic zones: from east to west, these are the Salcha seismic zone (Biswas and Tytgat, 1988), the Fairbanks seismic zone (Gedney *et al.*, 1980), and the Minto Flats seismic zone (Gedney *et al.*, 1972; Pulpan, 1986) (Fig. 2). In the mid-1980s, the Minto Flats seismic zone was considered the least defined of the three; as stated in Biswas and Tytgat (1988, p. 231): “The third seismic zone (Minto Flat seismic

^{*}Also at the Department of Geosciences, University of Alaska, 900 Yukon Drive, Fairbanks, Alaska 99775.

[†]Also at the Alaska Earthquake Center, University of Alaska, 903 Koyukuk Drive, Fairbanks, Alaska 99775.

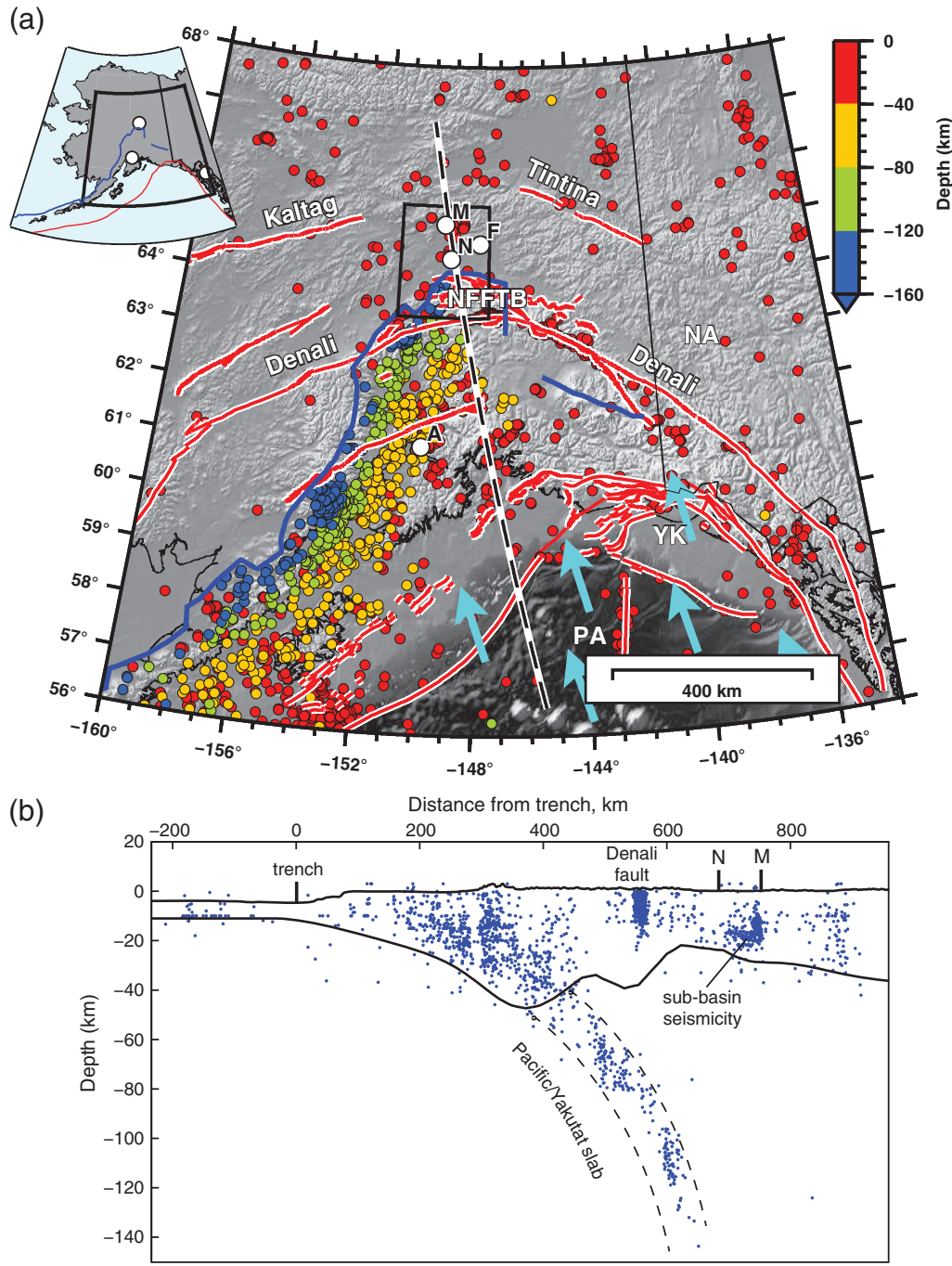


Figure 1. Active tectonic setting of Alaska. (a) Seismicity ($M \geq 4$, 1 January 1990–1 January 2015), plotted as colored circles, and active faults (Koehler *et al.*, 2012), including the Denali, Kaltag, and Tintina faults and the northern Foothills fold-and-thrust belt (NFFT). Open white circles: A, Anchorage, F, Fairbanks, N, Nenana, M, Minto; inset shows A and F. The box containing F, N, and M denotes the region of Figure 2 that contains the Minto Flats fault zone (MFFZ). Plates: NA, North America; PA, Pacific; and YK, Yakutat block. The arrows indicate PA motion relative to NA. The dark blue line marks the lateral extent of deep slab seismicity. (b) Seismicity profile ($M \geq 2.5$ within 30 km of the profile) along the dashed line in (a) with vertical exaggeration of 4:1. The MFFZ and Nenana basin are between Nenana (N) and Minto (M). The Moho model is from Wang and Tape (2014).

zone) of the greater Fairbanks area does not show a clear boundary... Rather, the earthquakes in this zone distribute in a diffused way and occasionally a felt earthquake ($M_L \approx 3.0$ to 4.0) is located along this zone.” However, the 1995 M_w 6.0 earthquake and subsequent aftershocks changed this perspective.

As described by Ratchkovski and Hansen (2002, pp. 1012–1013): “The Minto Flats seismic zone has the most coherent structure among the three major seismic zones in the interior and extends from the Kaltag fault in the north to the Kantishna cluster [of seismicity] in the south.”

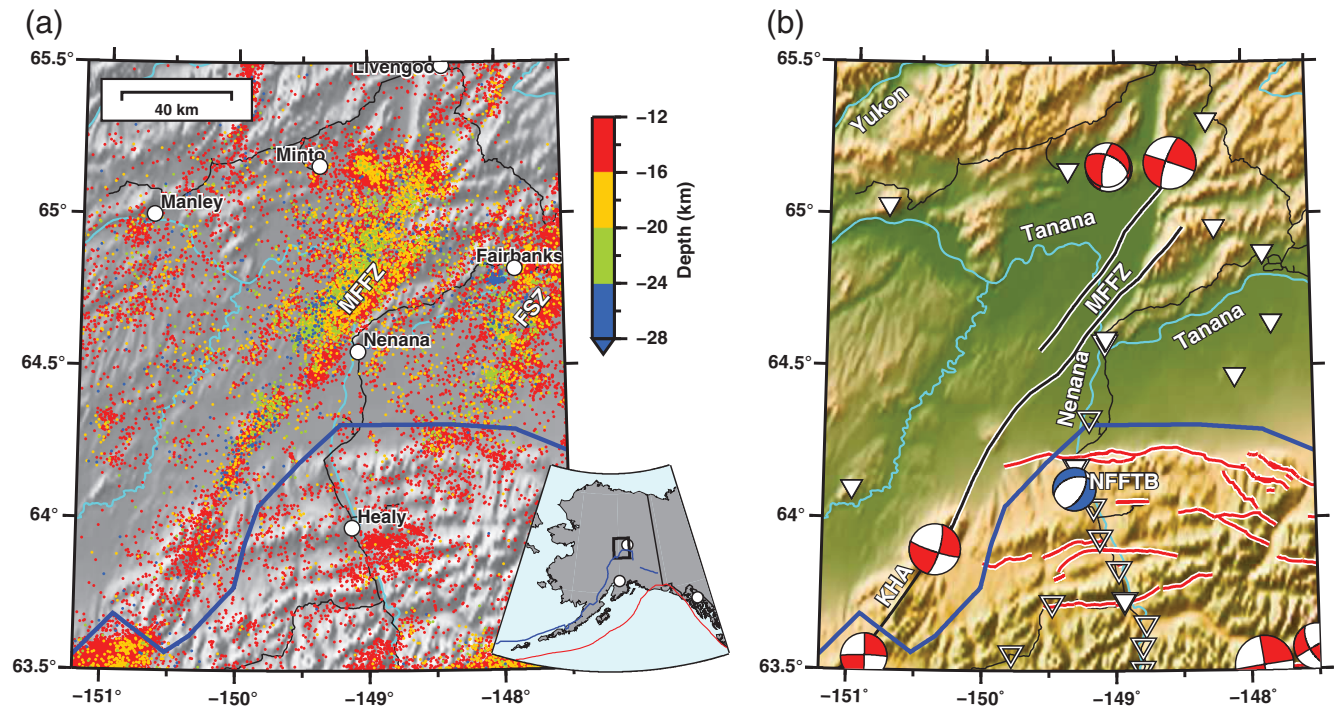


Figure 2. Crustal seismicity and station coverage in the MFFZ, central Alaska. The Nenana basin is situated above the seismically active region that defines the MFFZ (Fig. 4). (a) Seismicity from the Alaska Earthquake Center (AEC) catalog with $M > 0$, depth < 40 km, 1 January 1990–1 January 2015. Analysis of the seismicity reveals two lineaments (with deep crustal events) that define the MFFZ (Tape *et al.*, 2013). The Fairbanks seismic zone (FSZ) is also labeled; further to the east is the Salcha seismic zone, which produced the 22 July 1937 $M 7.3$ earthquake. The blue line marks the lateral extent of deep slab seismicity. (b) Broadband station coverage: permanent stations as of 1 September 2014 are plotted as white inverted triangles; Broadband Experiment Across the Alaska Range (BEAAR) stations from 1999 to 2001 are plotted as open inverted triangles. Many stations outside this region were also used in our study, including several BEAAR stations to the south. Active faults are plotted in red (Koehler *et al.*, 2012), notably the NFFTB. The Kantishna Hills anticline (KHA) is an active fold (Koehler *et al.*, 2012) that we do not consider to be part of the MFFZ (see also fig. 3 of Bemis *et al.*, 2012). The two seismic lineaments defining MFFZ are plotted in black with white outlines. Earthquake moment tensors are from the Global Centroid Moment Tensor (CMT) catalog (1 January 1976–1 January 2015) (Dziewonski *et al.*, 1981; Ekström *et al.*, 2012), including the 1995 $M_w 6.0$ Minto Flats earthquake. The moment tensors are plotted at the epicenters from the AEC catalog; the non-double-couple part of each Global CMT moment tensor is not plotted. Major rivers are labeled, with the Nenana River flowing north into the Tanana River, which flows west toward the Yukon River.

The Minto Flats seismic zone is an expression of multiple faults. Using seismicity catalogs from the 1990s, Page *et al.* (1995) noted that “activity is not confined to a single linear feature; thus, it intimates the possible presence of overlapping parallel faults, splays, and cross faults.” Ratchkovski and Hansen (2002) presented the first detailed examination of the Minto Flats seismic zone. Using focal mechanisms derived from first-motion polarity measurements and moment tensors derived from limited broadband data, they found that left-lateral strike-slip faulting predominated within the seismic zone. An analysis of the seismicity led Tape *et al.* (2013, their fig. S4) to identify two main lineaments, inferred as faults.

The Nenana sedimentary basin underlies the physiographic low-lying region of Minto Flats, through which the Tanana River flows (Fig. 2). The Nenana basin is approximately 90 km long and 12 km wide, with a maximum depth of 8 km (Van Kooten *et al.*, 2012). It is situated between (and above) the two seismic lineaments of the Minto Flats seismic zone. We refer to the seismic zone as the Minto Flats fault

zone (MFFZ) on the basis of seismological evidence in our study. However, there is no surface expression of the faults or evidence of Holocene fault scarps. Presumably the faults (and earthquake ruptures) do not extend to the surface or else they are covered by sediments.

In this study, we provide a comprehensive seismological analysis of the 180-km-long MFFZ. We relocate seismicity to define the two main faults within the zone, we characterize left-lateral faulting from new moment tensors, and we construct a finite-source model for the largest event within the fault zone over the past 30 years (1995 $M_w 6.0$). The coherence of seismicity and left-lateral faulting suggests that large earthquakes ($M_w \geq 7$) are possible within this fault zone. We find that the two major faults correspond with the margins of the Nenana basin. The current setting is one of the transtensional tectonics marked by a left-stepping strike-slip fault system, with a deep and narrow pull-apart basin between the two faults. This local transtensional setting is interpreted to have been active for the past 6 Ma, generating the tectonic subsidence to accommodate as much as 1.4 km of basin fill.

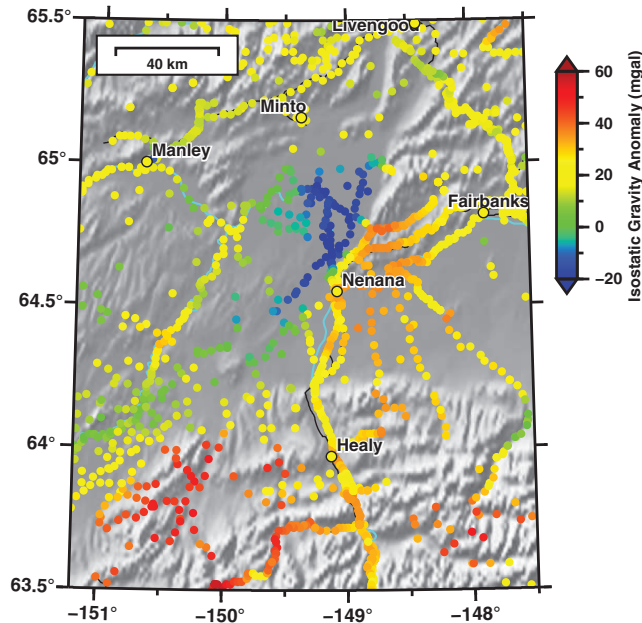


Figure 3. U.S. Geological Survey compiled gravity measurements in central Alaska, plotted as the isostatic gravity anomaly (Saltus *et al.*, 2008). The Nenana basin creates the gravity-low signature northwest of Nenana that was first identified by Barnes (1961). Almost all of the roads and rivers are covered by measurements.

The majority of the basin appears to have developed during an earlier episode of either local or regional extensional tectonics (Van Kooten *et al.*, 2012).

The Nenana Basin

The Nenana sedimentary basin, west of the town of Nenana, is described by Van Kooten *et al.* (2012) as “a structural half-graben with a large, normal basin bounding fault on the southeast margin. This fault forms an asymmetrical basin with a relatively steep southeast and a gentle northwest flank.” It was first identified based on a free-air gravity low (Barnes, 1961), and it is easily identified in regional gravity data sets (Fig. 3). The difficult access to the basin and its lack of bedrock have posed barriers to geological, seismological, and geophysical investigations. Recent exploration interests in the Nenana basin have led to industry seismic acquisitions and to new exploratory wells, including the Nunivak-1 well, drilled in 2009 to a depth of 3.4 km, and the Nunivak-2 well, drilled in 2013 to a depth of 2.6 km.

Using gravity data, Van Kooten *et al.* (2012) presented the first map of the topography of the Nenana basin basement surface. This preliminary surface, which covered the northern half of the basin, was later expanded (Doyon Limited, 2012) to cover the full basin, which is plotted in Figure 4. With a maximum depth of 8 km, the basin is one of the deepest in mainland Alaska. The basement surface provides the overall dimensions of the basin: about 90 km long and 12–15 km wide. Existing active-source seismic data were not used to constrain the basement surface (Doyon

Limited, 2012), and evidence from seismic cross sections of the basin (Van Kooten *et al.*, 2012) suggests that the western margin is not as steep as what is shown in Figure 4.

Core samples and well logs from Nunivak-1 and Nunivak-2 provide valuable data for interpreting the depositional history of the basin (Van Kooten *et al.*, 2012; Dixit and Hanks, 2014). Variations in lithology within the wells, as well as dates from palynology and microfossils, can be used to identify stratigraphic units that have been studied in exposed stratigraphic sections toward the Alaska Range (Wahrhaftig *et al.*, 1969; Ridgway *et al.*, 2007; Wartes *et al.*, 2013).

Figure 5 summarizes the stratigraphy in the Nunivak-1 well within the context of the tectonic history in the region. The stratigraphy marks four time intervals: (1) deposition from before 59 to 54.8 Ma, (2) an unconformity from 54.8 to 23.8 Ma, (3) deposition of the Usibelli group from 23.8 to approximately 6 Ma, and (4) deposition of the Nenana Gravel (and more recent sands and gravels) from 6 Ma to the present. Based on the 3.4 km at the base of Nunivak-1 and the maximum basin depth of 8 km, there are 4 km of undocumented sedimentary strata in the deepest parts of the basin. These strata could be some combination of (1) pre-59 Ma deposition associated with the foreland basin deposits within the lower Cantwell formation (Fig. 5) and (2) basinward thickening of the younger strata identified in the wells.

Seismic reflection data reveal a steep boundary at the eastern margin of Nenana basin (Ehm, 1983; Van Kooten *et al.*, 2012), consistent with the basement surface in Figure 4. This boundary appears to coincide with the seismic lineament (Fig. 2a) as well as with linear features within surface Holocene deposits in Minto Flats. Early geological studies identified a Minto fault that was correlated with seismicity (Péwé *et al.*, 1966; Gedney *et al.*, 1972). Recently Koehler *et al.* (2015) performed a targeted investigation of the surface features and concluded that the surface features marked an incised fluvial terrace, not a tectonic fault scarp. Several authors have inferred active tectonic deformation along the basin’s eastern margin based on fluvial geomorphology and morphometric analyses (Lesh and Ridgway, 2007; Frohman, 2014), but a positive link to an active fault at the surface has not been demonstrated.

Analysis of Seismicity within the Minto Flats Region

The MFFZ is a region of elevated seismicity and anomalously deep seismicity in central Alaska. Here we summarize some observations based on the seismicity from the Alaska Earthquake Center (AEC) catalog from 1 January 1990 to 1 January 2015; we restrict the depths to be ≤ 40 km to exclude slab events that are present to the south. During this time period, within the region of Figure 2 there were 31,848 crustal earthquakes, 6825 of which occurred within the MFFZ. The frequency–magnitude distribution implies a rate of $28 M \geq 2$ earthquakes per year and $1500 M \geq 0$ earthquakes per year (Fig. 6b).

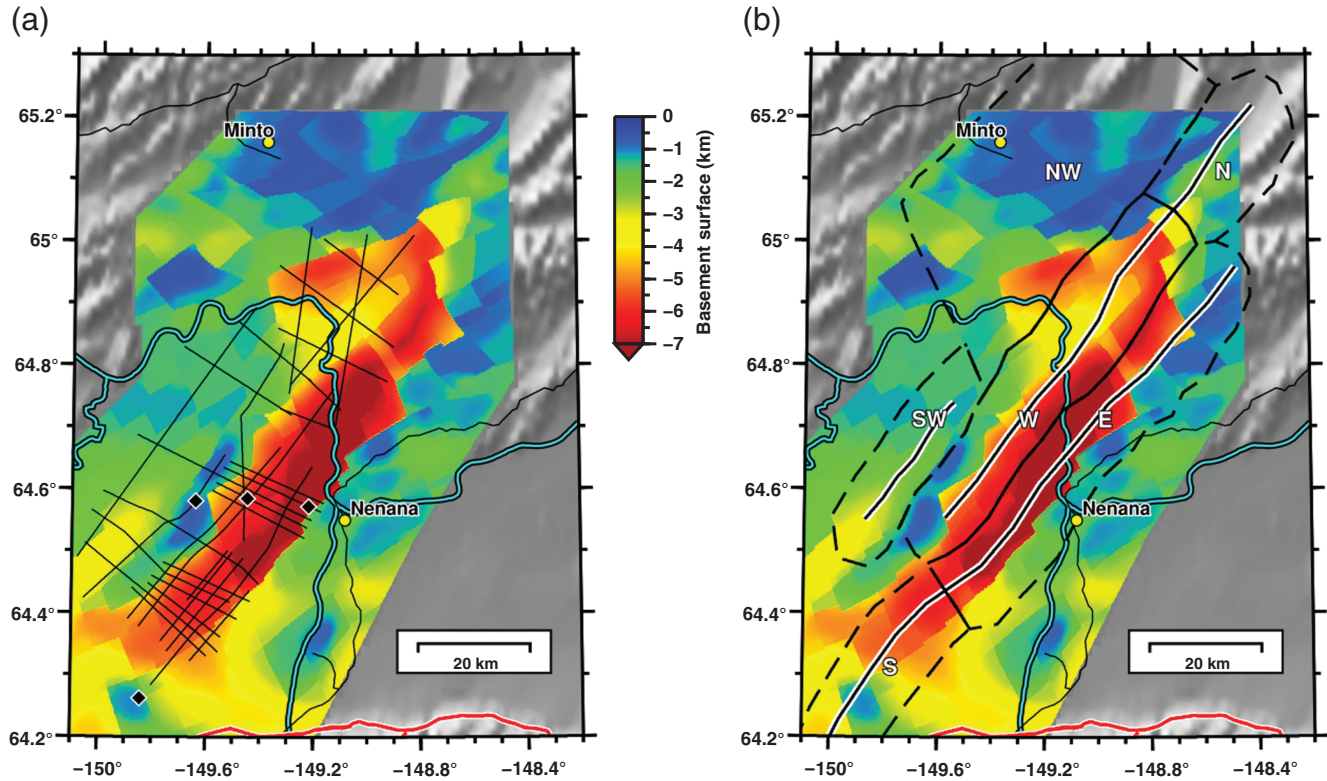


Figure 4. (a) Basement surface of the Nenana basin estimated from proprietary gravity and magnetic data (Doyon Limited, 2012). The maximum depth of the basement is 8.25 km and is between the two faults. The thin black lines show active-source seismic surveys in the region. The four black diamonds denote exploratory wells, including Nunivak-1 (2009) and Nunivak-2 (2013), the two closest to Nenana. The polygonal pattern in the basement surface is inferred from gradients in the gravity and magnetic data and is interpreted as basement-faulted blocks; however, there is little evidence for these features in the seismic reflection data (Van Kooten *et al.*, 2012). (b) Subregions of the MFFZ used for analysis of seismicity and focal mechanisms. Subregions N (north), W (west), E (east), S (south), and SW (southwest) are considered part of the MFFZ. We also analyze some recent events in the northwest (NW) subregion (Table 1), but we do not consider this subregion part of the MFFZ. The thick black lines are the seismic lineaments (interpreted as faults) derived from earthquake data.

We analyze seismicity and significant earthquakes within subregions based on two main lineaments mapped in figure S4 of Tape *et al.* (2013) and also on two zones adjacent to and northwest of the main two lineaments (Fig. 4). There are four subregions along the main fault zone. The west (W) and east (E) subregions encompass the zone of overlap between the two strands, and the north (N) and south (S) subregions are extensions of the faults. We include a subregion to the west (labeled southwest [SW]) that is visible as a seismic lineament in figure S4 of Tape *et al.* (2013). We include the northwest (NW) subregion for comparison; although we do not consider this subregion part of the MFFZ, it has produced several $M_w > 4$ earthquakes, including four in 2014 that are listed in Table 1. (E) The electronic supplement contains figures of the frequency–magnitude distributions and depth distributions for each subregion (Figs. S4 and S5).

The MFFZ contains markedly deeper earthquakes, with a median depth of 14.9 km compared with 11.0 km for the entire region (Fig. 6c). Earthquakes within the MFFZ occur at greater depths in the western subregion (1930 events; median 16.7 km) than in the eastern subregion (2599 events; median 14.2 km) (Fig. 6d). Earthquakes occur throughout the lower crust and perhaps to the base of the crust or within

the uppermost mantle. For example, the crustal thickness is estimated to be <30 km (Beaudoin *et al.*, 1992; Veenstra *et al.*, 2006; Wang and Tape, 2014), and about 5% of events in the western subregion occur below 24 km (Fig. 6d).

Relocation of Seismicity

To better understand the patterns identified from the seismicity catalog, we relocate the events in the vicinity of the MFFZ using the double-difference method of Waldhauser and Ellsworth (2000) (*hypoDD* 2.1b). In this method, travel-time differences for event pairs recorded at common stations are used to locate the earthquakes relative to each other. We use both *P* and *S* picks of earthquakes in the AEC earthquake catalog from 1975 to 2014. Although previous studies have relocated earthquakes in central Alaska (e.g., Ruppert *et al.*, 2008), this is the first time that waveform cross-correlation data have been incorporated in the procedures. Cross correlations are used to provide a correction to the travel-time differences calculated from the catalog data, so we are concerned only with aligning the initial arrival of the phases. Correlation data are used for events that meet a minimum correlation value of 0.70 over a correlation window of

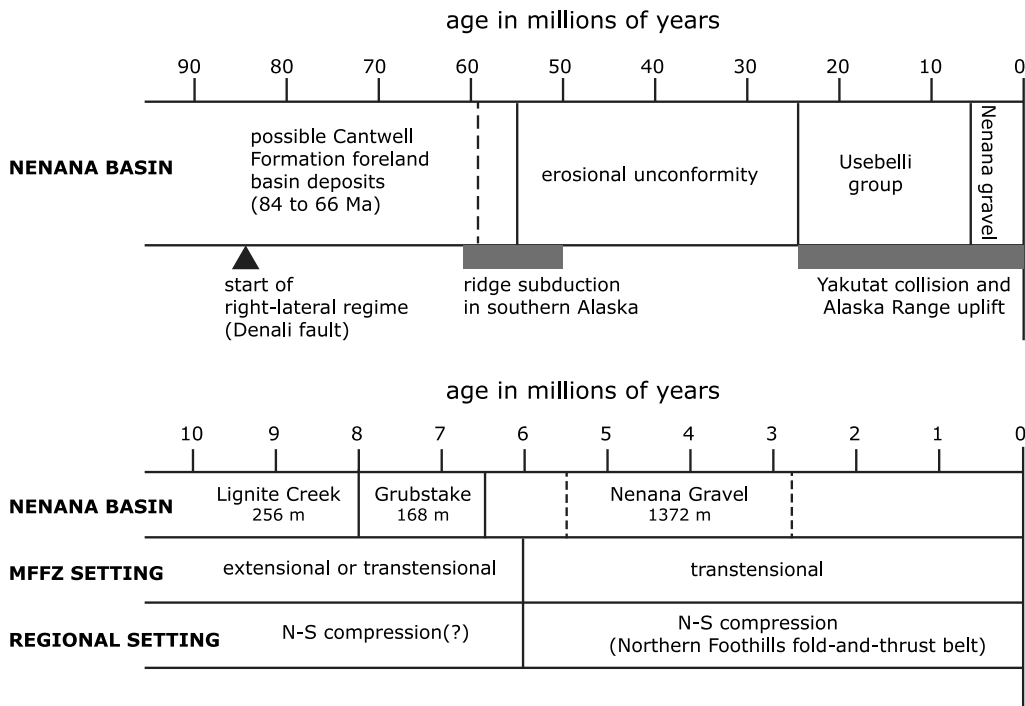


Figure 5. Stratigraphic time scale for the Nenana basin, based on the results from the Nunivak-1 well (Van Kooten *et al.*, 2012). (top) The base of Nunivak-1, marked by the vertical dashed line, is within Late Paleocene sedimentary strata. The unknown strata between the well bottom and the crystalline basement are possibly the lower Cantwell formation (late Campanian to early Maastrichtian) (Ridgway *et al.*, 1997). An erosional unconformity spans 31 Ma, from 54.8 to 23.8 Ma (Van Kooten *et al.*, 2012). The right-lateral strike-slip fault regime includes the Denali fault and initiated around 85 Ma (Miller *et al.*, 2002). Two episodes of perturbation to subduction in southern Alaska are labeled as ridge subduction at 61–50 Ma (Marshak and Karig, 1977; Bradley *et al.*, 2003; Haeussler *et al.*, 2003) and the Yakutat collision at 24 Ma, which coincided with uplift of the Alaska Range (Benowitz *et al.*, 2011, 2014). (bottom) Expanded view of the last 10 Ma. The uppermost formations of the Usibelli group are Lignite Creek and Grubstake. The temporal boundaries of the Grubstake formations are identified by Wahrhaftig *et al.* (1969), Leopold and Lu (1994), and Triplehorn *et al.* (2000). The time range for the Nenana gravel from Ager *et al.* (1994) is marked by the vertical dashed lines (5.4–2.9 Ma). The date of the latest Nenana gravel deposits is debatable (Ridgway *et al.*, 2007); for our purposes, we consider the last ~6 Ma (marking the uppermost strata in Nenana basin from the top of the Grubstake formation to the surface) to be Nenana gravel plus more recent fluvial deposits.

1.0 s. Initially we used the same 1D velocity model used by the AEC to locate events in central and northern Alaska (Huang and Biswas, 1983), with V_S uniformly scaled from V_P as $V_S = V_P/1.78$. Because of the presence of the Nenana basin in this region, we reduce the P velocity of the uppermost layer (by 1 km/s) to 4.9 km/s. (All stations are outside the basin, so we do not assign the uppermost layer to be as slow as the basin itself.)

A subset of the relocated catalog is plotted in Figure 7b in comparison with the AEC catalog (Fig. 7a). The two main faults of the MFFZ are better delineated in the relocated seismicity. The results from Figure 6d, showing that earthquakes on the western fault are deeper than those on the eastern fault, are visible in the map of the relocated catalog (Fig. 7b). The relocated catalog provides a clearer picture of the possible fault patterns within the northern subregion, which contains the 1995 M_w 6.0 earthquake and its aftershocks. In this region, there is a northwest–southeast spread of seismicity that suggests the possibility of a fault that runs approximately perpendicular to the trend of the MFFZ. These events tend to occur at shallower depths (<12 km) than those in the MFFZ.

Moment Tensors Derived from Body Waves and Surface Waves

A primary goal of this study is to characterize the style of faulting within the MFFZ by analyzing the best-recorded earthquakes. Using the boundaries shown in Figure 4, we identify the largest-magnitude events within each subregion over the time period 1 January 1999 to 31 July 2014; the start time of this interval marks the approximate start of the broadband instrument era in Alaska. We perform moment tensor inversions for all events with at least 10 stations with waveforms having good signal-to-noise ratios. Our final set of 11 events within MFFZ is listed in Table 1.

We use broadband waveforms from the permanent network in Alaska, as well as those from temporary arrays, when available. For events in 1999–2001, we use stations from the Broadband Experiment Across the Alaska Range (BEAAR) array, which provides excellent coverage for paths to the south. These stations were not available for the analysis of Ratchkovski and Hansen (2002), and they significantly reduce the uncertainties of moment tensors in MFFZ. Broadband station coverage in central Alaska has steadily

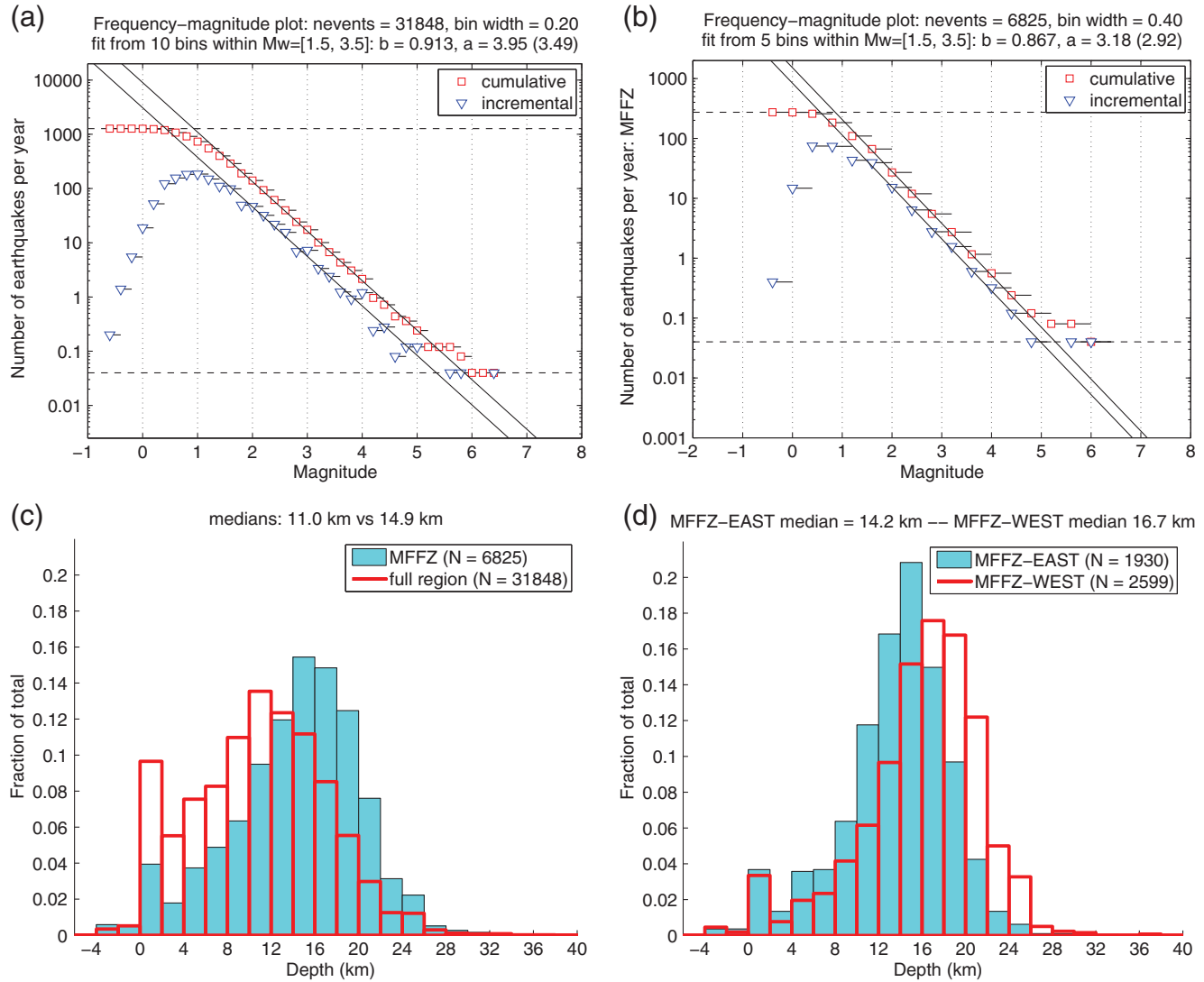


Figure 6. Analysis of crustal seismicity in the region of Minto Flats, using the AEC catalog, $M \geq 0$, 1 January 1990–1 January 2015, depths ≤ 40 km (nevents is the number of events). (a) Frequency–magnitude distribution for the region of Figure 2. (b) Frequency–magnitude distribution for the combined five subregions in Figure 4. (c) Comparison of depths of events for the region of Figure 2 and for the combined five subregions. Events in the MFFZ are generally deeper than those in the surrounding region. (d) Comparison of depth of events for the west and east subregions. Events in the west subregion of the MFFZ are somewhat deeper than those in the east subregion.

increased since 2000, so the events with the best coverage are the most recent (Table 1, Fig. 2b).

We estimate moment tensors by using body waves and surface waves and by searching over the model parameter space of strike angle (0° to 360°), dip angle (0° to 90°), rake angle (-90° to 90°), magnitude, and depth (Zhu and Helmberger, 1996) (Table 1). For some events, we use a limited number of polarity measurements to reduce the solution space over which waveform fitting is applied (Table 1). We assume a double-couple model for all moment tensors.

Figure 8 shows selected waveform fits for the 29 November 2000 M_w 5.7 earthquake (event A in Table 1) in the southern subregion of the MFFZ. The full solution (Fig. S2a) uses 21 stations, mostly from the BEAAR temporary array (e.g., Ferris *et al.*, 2003). We were unable to use surface waves from

the closest stations due to contamination from an aftershock that occurred about 40 s after the M_w 5.7 event (e.g., Ratchkovski and Hansen, 2002). Nevertheless, there are excellent waveform fits for this event. If the fault plane is assumed to be north-to-northeast striking, the fault is oriented with strike 10° and dip 82° (east), and the mechanism is pure strike slip (rake 0°).

Our moment tensor solutions reveal the prevalence of left-lateral faulting within all five subregions of the fault zone (Fig. 9). Fits between synthetic and observed waveforms are presented in Figure S2. In Figure 10, we compare our results with Ratchkovski and Hansen (2002) and existing catalogs. In general, the pattern of left-lateral faulting is more consistent in our set of events than in other compilations.

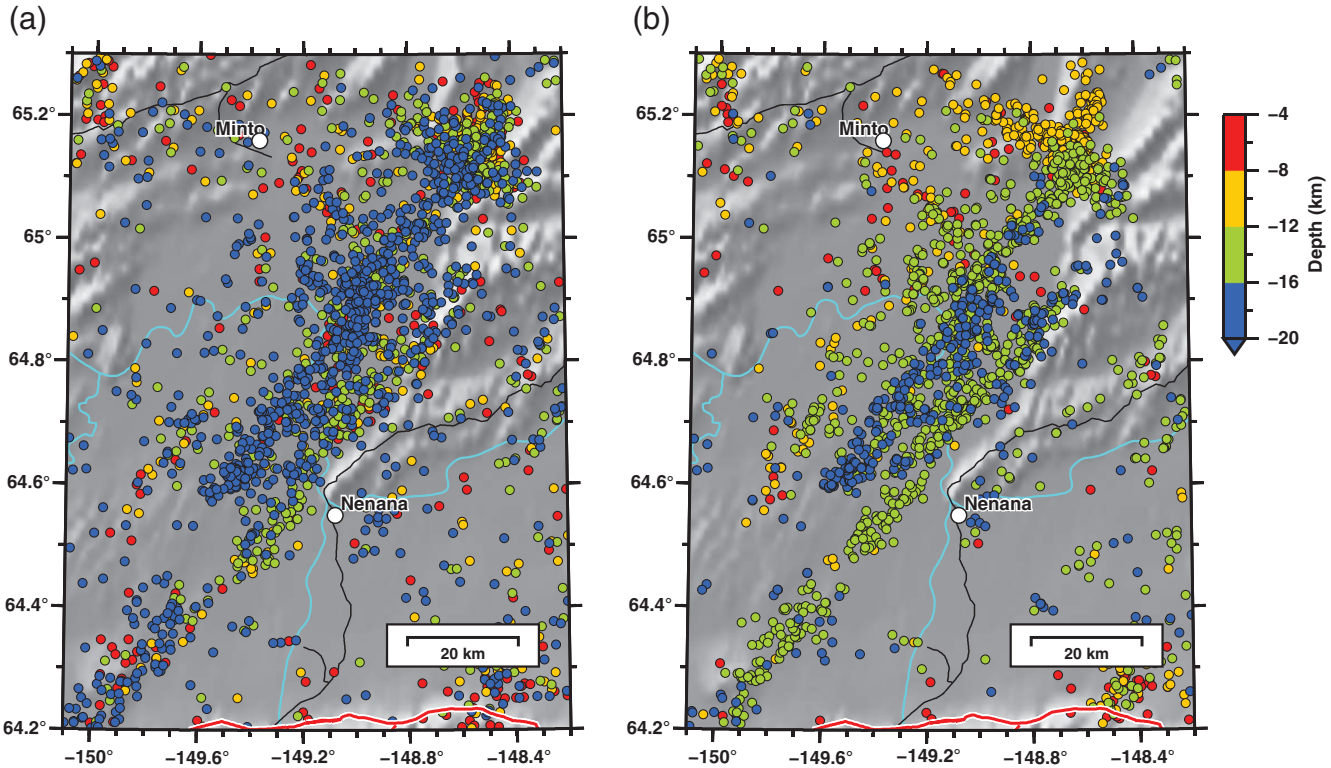


Figure 7. Earthquake relocations using waveform cross correlation. Here the catalog parameters are $M \geq 1.5$, 1 January 1990–31 December 2012. (a) AEC catalog. (b) Relocated catalog from this study. Notice the depth-dependent difference between the two faults, with the western fault experiencing deeper events (> 16 km) than the eastern fault.

Table 1
Moment Tensor Solutions in This Study

Event*	Origin Time (yyyy/mm/dd hh:mm:ss.sss)	Subregion [†]	Latitude (°)	Longitude (°)	Strike (°) [‡]	Dip (°)	Rake (°)	M_w	Depth	Nsta [§]	Npol
A	2000/11/29 10:35:47.240	S	63.90	-150.35	10	83	0	5.7	19 (16.4)	21	3
B	2000/12/06 18:40:26.044	S	63.89	-150.31	10	83	0	4.9	10 (11.7)	18	4
C	2001/03/25 11:34:50.863	E	64.63	-149.25	230	68	10	4.4	20 (22.2)	14	1
D	2001/06/30 09:41:42.263	S	64.04	-150.15	200	83	10	4.6	16 (14.6)	22	0
E	2008/07/16 10:12:00.620	W	64.59	-149.53	30	68	40	3.9	23 (30.5)	25	0
F	2009/07/28 12:13:15.710	W	64.61	-149.49	30	68	-10	3.8	23 (22.7)	13	0
G	2012/04/11 09:21:57.444	W	64.92	-148.95	190	76	-40	3.9	16 (19.3)	14	6
H	2013/03/05 21:55:58.372	E	64.84	-148.73	210	83	0	3.4	20 (17.3)	18	0
I	2013/06/05 18:58:23.293	SW	64.64	-149.68	210	83	-20	3.9	10 (13.9)	22	0
J	2013/07/12 07:59:17.004	N	65.09	-148.77	30	83	10	3.6	16 (17.2)	24	1
K	2014/12/13 15:47:31.423	E	64.43	-149.38	150	52	-60	3.4	17 (13.0)	17	0
L	2014/08/31 03:06:57.111	NW	65.15	-149.04	200	76	-30	5.0	12 (16.0)	52	1
M	2014/08/31 12:24:58.258	NW	65.16	-149.05	200	83	-20	4.1	16 (16.0)	47	1
N	2014/10/21 00:36:58.333	NW	65.15	-149.04	190	68	-10	4.7	13 (18.0)	51	1
O	2014/10/23 16:30:23.968	NW	65.16	-149.05	200	76	-30	4.8	13 (17.0)	60	1
	1995/10/06 05:23:18.960	N	65.1586	-148.5422	199	77	-1	6.0	17 (12.2)	—	—

*Event G is a slightly revised solution from the one presented in Tape *et al.* (2013). Events L–O are in the northwest subregion, which is not considered part of the Minto Flats fault zone (MFFZ). For the last event listed, the hypocenter and origin time are from Ratchkovski and Hansen (2002), the magnitude and fault angles are from the Global Centroid Moment Tensor catalog, and the depth is estimated from the main slip patch in Figure 11. The event ID is derived from the catalog origin time.

[†]The subregion corresponds to the designation in Figure 4b.

[‡]The strike, dip, and rake angles uniquely define the moment tensor orientation (Tape and Tape, 2012); however, the fault plane and slip vector could be associated with one of two sets of angles. The dip angle is measured in a right-handed convention based on the strike direction. The depth is from the moment tensor inversion, with the catalog depth in parentheses.

[§]Nsta, number of stations used.

^{||}Npol is the number of first-motion polarity measurements used.

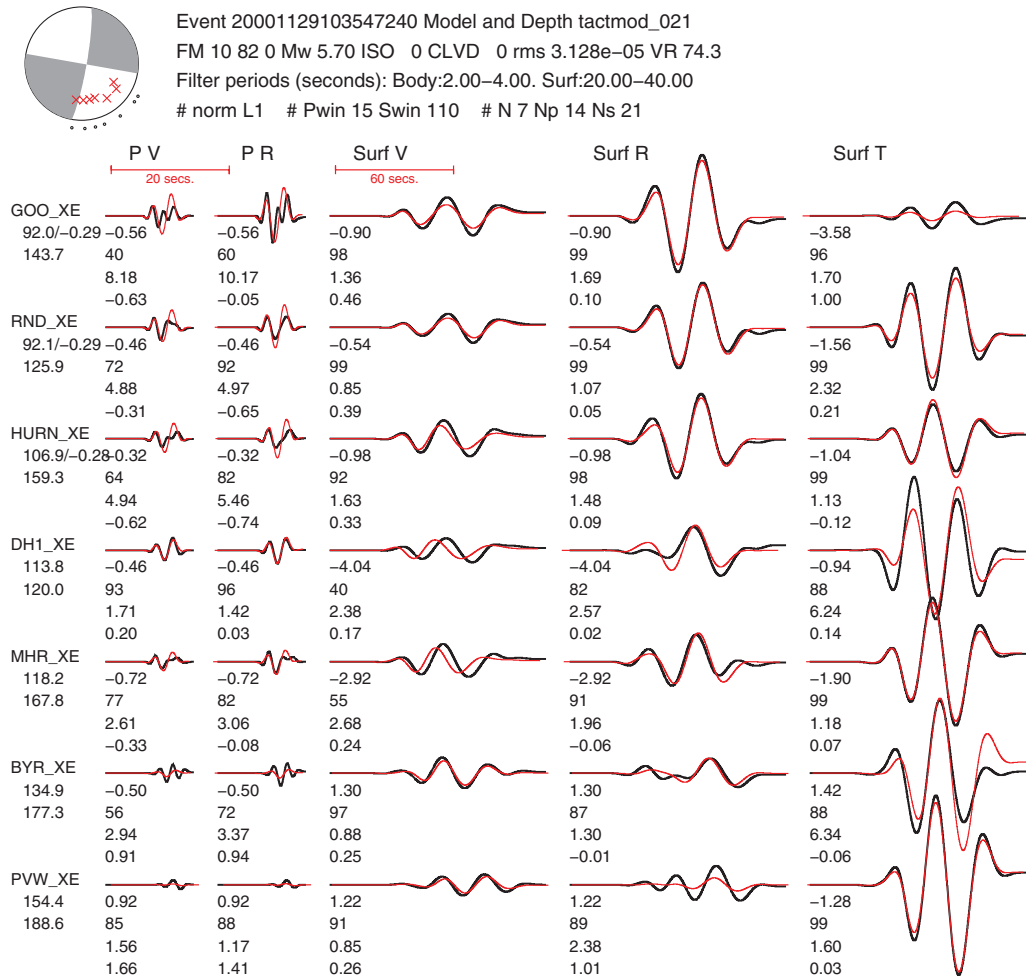


Figure 8. Selected waveform fits for the 29 November 2000 M_w 5.7 earthquake in the southern end of the MFFZ (event A of Table 1). (E) For waveform fits from all stations, see Figure S2a. Searching over depth gives a best fit of 21.0 ± 5.2 km (E Fig. S3a), which is shallower than the depth of 43.7 km listed in the Global CMT catalog but consistent with the depths in the AEC catalog (16.4 km) and in Ratchkovski and Hansen (2002) (19.5 km).

One event, event K, is a clear normal-fault mechanism that occurred at a depth of 17 km (Fig. 9b). Within our analysis, this small (M_w 3.4) but well-constrained mechanism is the best example of non-strike-slip faulting. Interestingly, neither of its possible fault planes is consistent with it occurring on one of the main faults within the fault zone. It is located at the southern end of the deepest part of the basin and slightly east of the seismicity-defined fault (Fig. 9b). In the context of transtensional tectonics (see the Discussion section), event K may represent secondary extensional faulting that promotes basin subsidence.

Finite-Source Model for the 1995 M_w 6.0 Minto Flats Earthquake

The 6 October 1995 M_w 6.0 earthquake in Minto Flats provides further support for the MFFZ as a left-lateral fault system (Ratchkovski and Hansen, 2002). Here we use teleseismic recordings of this event to determine a finite-source model for the earthquake. The Global Centroid Moment Ten-

sor for this earthquake (Fig. 2b) provides the possibility for a northeast–southwest fault plane or a northwest–southeast fault plane. Our analysis of double-difference aftershock locations (see E the electronic supplement) corroborates the findings of Ratchkovski and Hansen (2002) of a steep fault plane striking northeast–southwest. We assume a fault plane that strikes 200° and dips 80° to the west, based on moment tensor solutions for the mainshock and four aftershocks in Ratchkovski and Hansen (2002). The northwest–southeast (auxiliary) plane provides a poor fit to the observed waveforms, as shown in E Figure S7.

The 1995 M_w 6.0 Minto earthquake occurred on 6 October at 05:23:19 UTC (Ratchkovski and Hansen, 2002). The finite-source inversion for this earthquake is challenging due to the occurrence of an M_w 5.8 earthquake near Jalisco, Mexico, which initiated 10 min earlier. The Jalisco waveforms overprint the 1995 Minto earthquake waveforms at many stations. We were only able to use 6 P waves and 11 S waves with relatively high signal-to-noise ratios. The azimuthal coverage is very limited, particularly for P waves

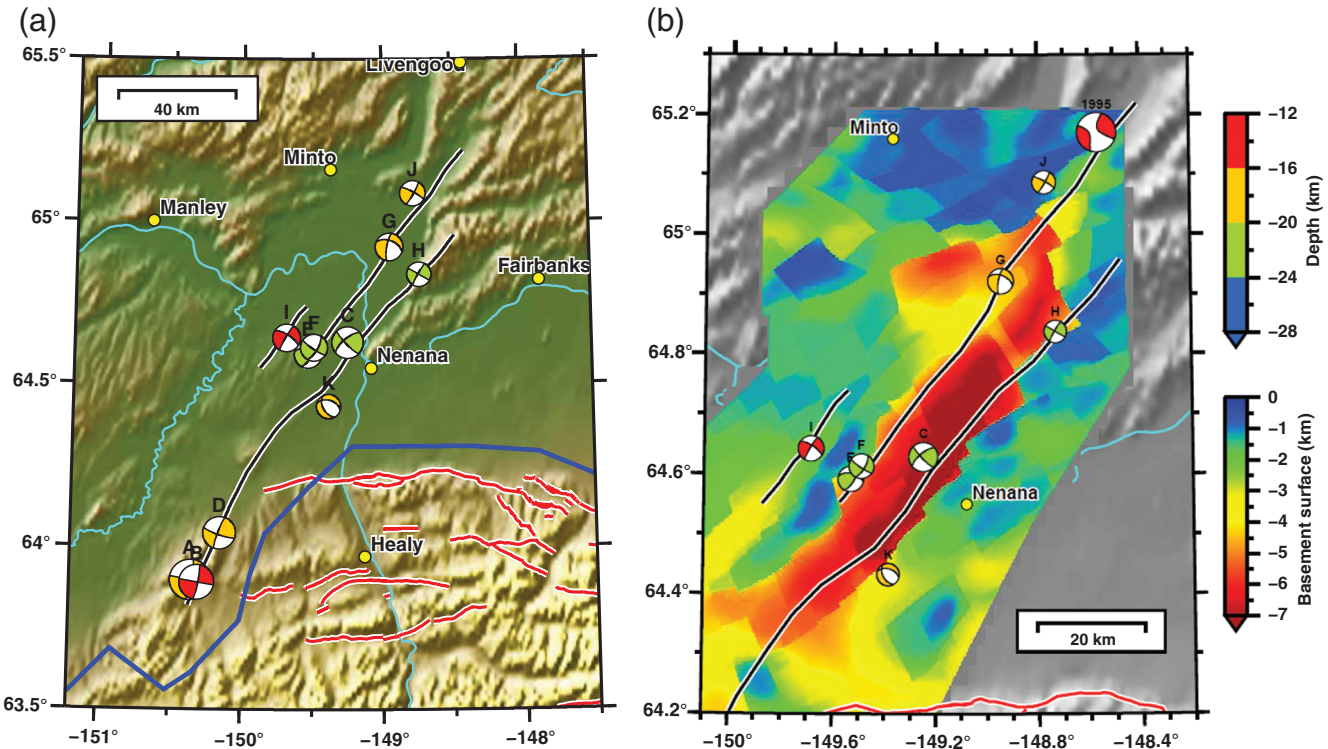


Figure 9. Moment tensors from this study (Table 1), revealing the dominance of left-lateral faulting in the MFFZ. Beachballs are colored according to depth using the scale at upper right. (a) Full region. (b) Enlarged region, with the Nenana basin basement surface plotted for reference (scale at lower right). The Global CMT moment tensor for the 1995 M_w 6.0 earthquake, plotted at the epicenter from the AEC catalog.

(Fig. 11). The velocity data have been band-pass filtered between 0.005 and 1 Hz and integrated to displacement. The synthetic seismograms are calculated using a first-motion approximation (Langston and Helmberger, 1975). The attenuation parameter used in this study is $t^* = 0.7$ s for P waves and 3.5 s for SH waves. The 1D Alaska velocity model tactmod (Beaudoin *et al.*, 1992; Ratchkovski and Hansen, 2002) is used to model the earth response near the source.

We approximate the causative fault geometry with a $30 \text{ km} \times 20 \text{ km}$ rectangular fault plane striking 200° and dipping 80° . The fault plane is further divided into 600 subfaults with dimensions $1 \text{ km} \times 1 \text{ km}$. We adopt a simulated annealing method to simultaneously invert for slip amplitude, rake angle, rupture initiation time, and the shape of an asymmetric function for each subfault. The inverted parameters are obtained by finding the best match in the wavelet domain between the computed synthetics (based on the source parameters) and the strong-motion waveforms (Ji *et al.*, 2002, 2003). The slip amplitude varies from 0 to 100 cm and rake angle changes from -30° to 30° . We allow the starting time and end time of the asymmetric slip rate function (Ji *et al.*, 2003) to range from 0.1 to 1.0 s. The value of rise time was therefore limited to lie between 0.2 and 2.0 s. We let rupture initiate at the relocated hypocenter (Ratchkovski and Hansen, 2002). The rupture initiation time of each subfault changes within $[L/v_{\text{ref}} - \tau, L/v_{\text{ref}} + \tau]$, in which L is the on-fault distance

to the hypocenter and v_{ref} is the average rupture velocity (Shao *et al.*, 2011). v_{ref} and maximum perturbation time τ used during final inversion are 2.5 km/s and 3 s, respectively. We stabilize the inversion by applying the Laplace smoothing constraints to the inverted fault slip and the rupture initiation time (Shao *et al.*, 2011).

The preferred fault model for the 1995 Minto earthquake has a cumulative seismic moment of $1.0 \times 10^{18} \text{ N}\cdot\text{m}$ (M_w 5.93) during its 8 s of coseismic rupture. The peak slip is 57 cm. Although we used 600 subfaults, the slip model is compact. Only one-fourth of subfaults have slip larger than 10% of the peak slip. These subfaults have an average slip of 17 cm and are responsible for about 87% of the total seismic moment. The earthquake has two dominant slip patches. The rupture initiated at the center of the largest slip patch and propagated bilaterally, mainly along the vertical direction. This slip patch spans 4 km along strike but extends from about 9 to 19 km in the downdip direction. The second largest slip patch has a dimension of 4 km along strike and 5 km downdip. Its centroid is located 6 km north-northeast of the hypocenter and at a depth of 8 km. Its rupture initiated at about 2.5 s and produced the second highest peak in moment rate function (Fig. 11b). Its peak slip is 47 cm.

The coincidence in time of the M_w 5.8 Jalisco earthquake waveforms with the origin of the M_w 6.0 Minto earthquake raises the possibility that the Minto earthquake was

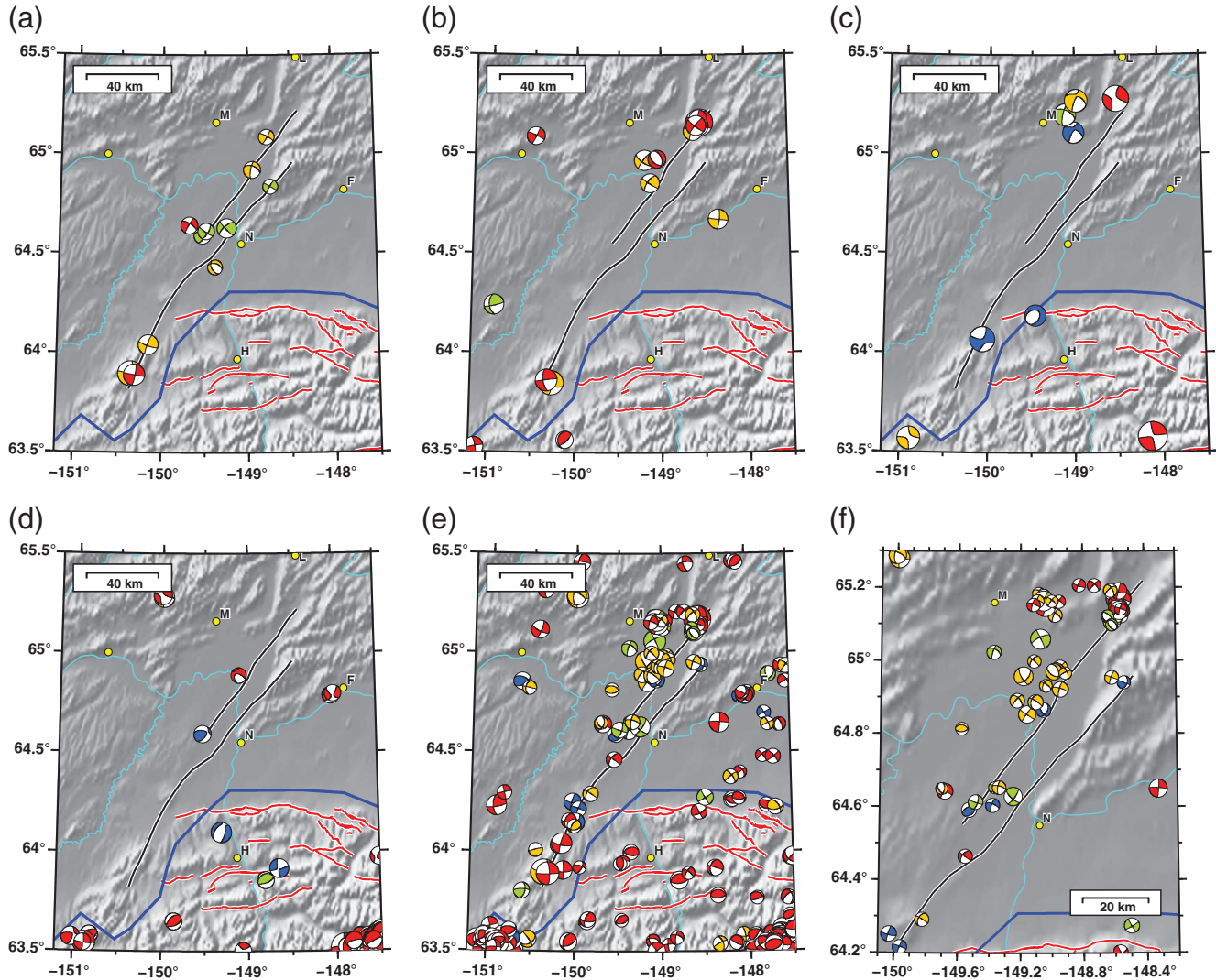


Figure 10. Comparison of our moment tensors with those from other catalogs and studies. The color scale for depth is shown in the upper right of Figure 9b. The blue line marks the lateral extent of deep slab seismicity. Towns are plotted for reference: H, Healy; N, Nenana; M, Minto; L, Livengood; and F, Fairbanks. Events are as follows: (a) this study, 1 January 2000–1 January 2015; (b) Ratchkovski and Hansen (2002), 1989–2000; (c) Global CMT catalog, 1 January 1976–1 January 2015; (d) the complete AEC moment tensor catalog (21 October 2002–31 March 2014); (e) AEC first-motion catalog, 1 January 1988–1 January 2015 (this is a subset of events for $M \geq 3$); and (f) same as (e), but zoomed in on the MFFZ.

dynamically triggered. Figure 12a shows the vertical-component velocity seismogram at station COL in Fairbanks, 47 km from the epicenter. A zoom-in or high-pass-filtered version reveals that the high-frequency waves from the Jalisco earthquake arrived in the Minto Flats epicenter region at about 30 s prior to the initiation of the Minto earthquake. In other words, the M_w 6.0 Minto Flats earthquake initiated during the coda of the P wave from the Jalisco earthquake. A separate event (event G in Table 1) was dynamically triggered by Love waves from the M_w 8.6 Indian Ocean earthquake (Hawthorne and Ampuero, 2013; Tape *et al.*, 2013). Both the 1995 M_w 6.0 Minto earthquake and the 2012 M_w 3.9 event G earthquake occurred on the western fault within the fault zone and at a depth of 15–20 km. It is pos-

sible that the MFFZ is susceptible to dynamic triggering and that the 1995 Minto earthquake was triggered.

Discussion

The MFFZ and Nenana basin should be examined over a range of spatial and temporal scales. At the largest spatial scale, the active tectonics of Alaska are driven by subduction and collision of the Pacific–Yakutat slab (Plafker and Berg, 1994; Haussler, 2008). Convergence between the Pacific plate and North America spans most of Alaska, as manifested by seismicity and GPS measurements (Freymueller *et al.*, 2008; Leonard *et al.*, 2008). Stress patterns inferred from focal mechanisms and strain rates derived

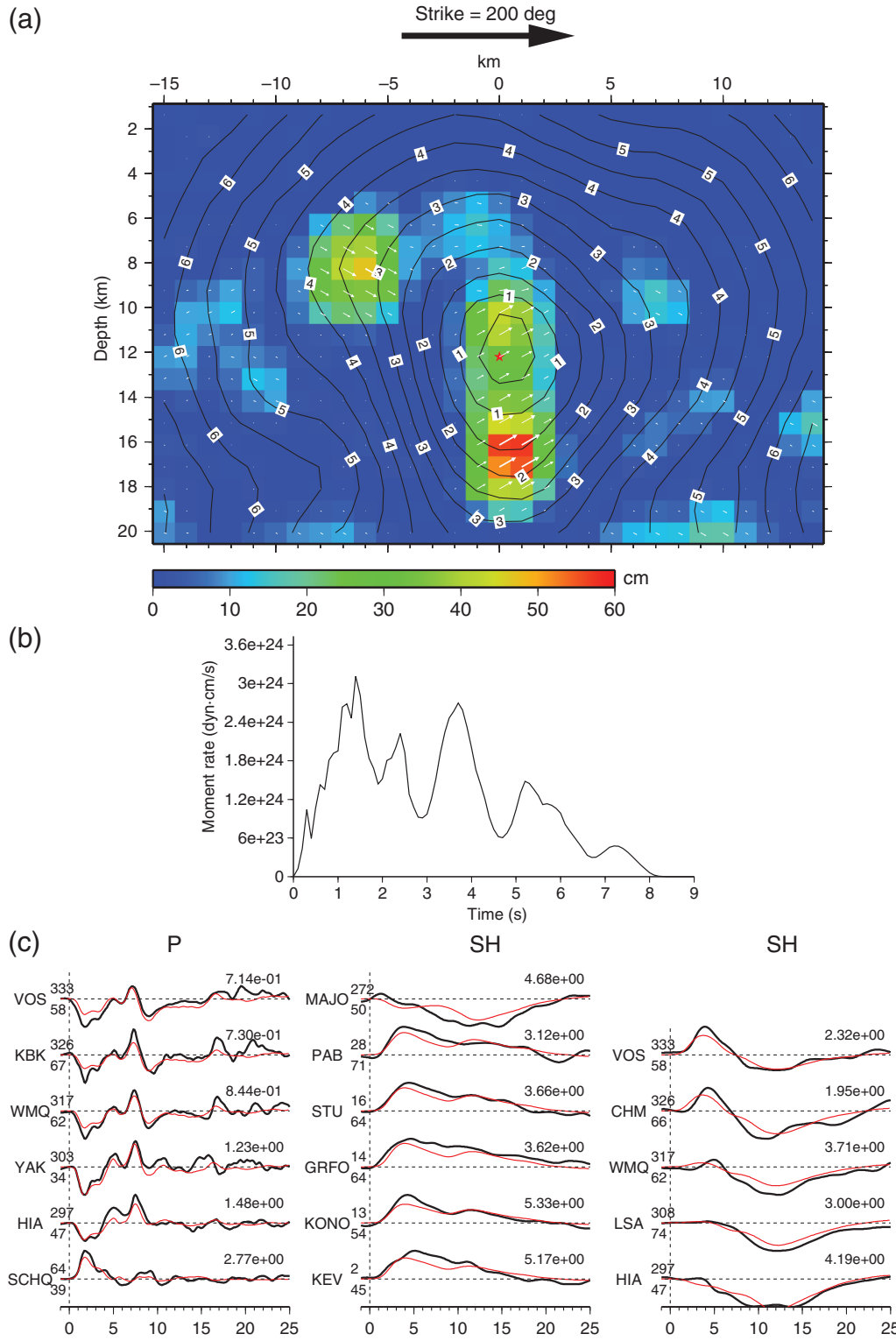


Figure 11. Finite-slip inversion model for the M_w 6.0 earthquake in Minto Flats. (a) Cross section of the slip distribution. The direction of the view is toward the east (azimuth 110°). The red star indicates the hypocenter, the color denotes the slip amplitude, and black contour lines indicate the rupture time in seconds. (b) Moment rate function. This is the sum of the moment rate functions for all subfaults, with each moment rate function time-shifted by its onset time. (c) Comparison of observed teleseismic P and SH wave waveforms (black lines) and synthetic seismograms (red lines). For each comparison, the value above the beginning of the trace is the station azimuth relative to the epicenter and the value below is the epicentral distance. The value above the end of the trace is the observed peak amplitude in micrometers per second, which is used to normalize the synthetic and observed seismograms. Few stations are available for this inversion, due to the interference from an M_w 5.8 earthquake near Jalisco, Mexico (Fig. 12).

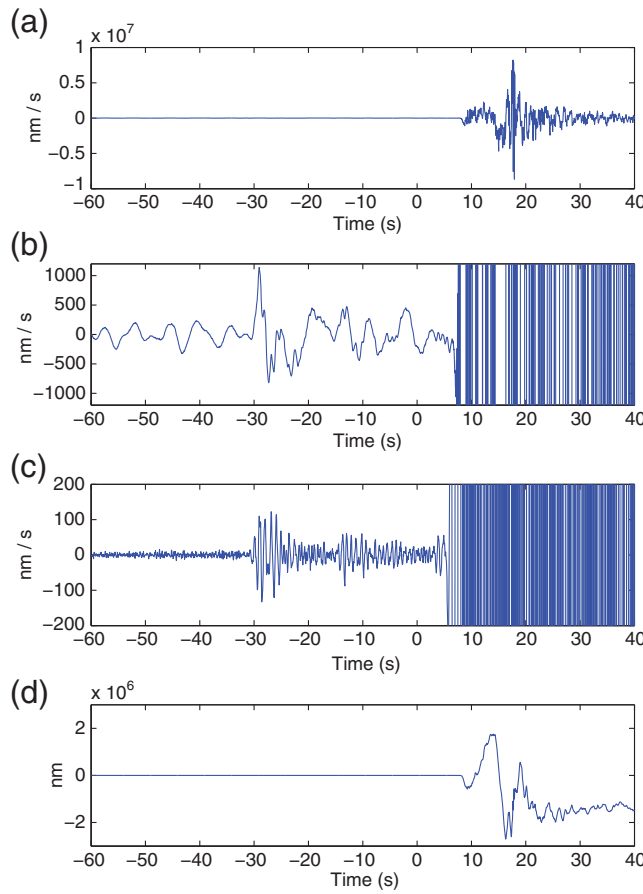


Figure 12. The seismogram at station COL for the 1995 M_w 6.0 earthquake in Minto Flats. The origin time of the event is at $t = 0$ s, which is 6 October 1995 05:23:18.96 UTC. (a) Velocity seismogram in nanometers per second. (b) Enlarged view of (a), showing the presence of waveforms from an M_w 5.8 earthquake near Jalisco, Mexico. (c) High-pass-filtered version ($f \geq 1$ Hz) of the seismogram in (b). (d) Integrated version of (a). This vertical displacement time series, as well as the horizontal displacement time series, indicate clipping at COL for this earthquake.

from GPS measurements leave open the possibility for numerous interpretations of schematic models or deformation models for how mainland Alaska is accommodating convergence (Redfield *et al.*, 1997; Mazzotti and Hyndman, 2002; Ratchkovski and Hansen, 2002; Freymueller *et al.*, 2008; Fuis *et al.*, 2008; Haeussler, 2008; Ruppert, 2008; Koons *et al.*, 2010; Finzel *et al.*, 2011).

At the scale of central Alaska, the tectonic setting is one of convergence, manifested by active strike-slip and thrust-fault systems. There are two large-scale right-lateral fault systems of Denali (to the south) and Kaltag–Tintina (to the north), with an active fold-and-thrust belt just north of the Denali fault (Bemis and Wallace, 2007; Bemis *et al.*, 2012) (Fig. 1). Between these right-lateral faults is a series of north-east-striking seismic lineaments that exhibit predominantly left-lateral faulting, one of which is the MFFZ (Ratchkovski and Hansen, 2002; Ruppert *et al.*, 2008).

Several conceptual models have been proposed for the pattern of faulting and deformation in central Alaska (Haeussler, 2008), such as block rotation within the right-lateral shear zone to accommodate left-lateral faulting (Page *et al.*, 1995). Cross and Freymueller (2008) and Ruppert *et al.* (2008) suggested that the MFFZ could be related to rotation of the Bering plate (Mackey *et al.*, 1997) and serves as its eastern boundary. According to the latest perspectives, the most likely mechanisms driving shear in the interior are a combination of north-south compression generated from counterclockwise rotation and northward migration of the southern Alaska block, together with internal shortening in the Alaska Range (Haeussler, 2008; Frohman, 2014; Haeussler *et al.*, 2014; Bemis *et al.*, 2015).

A temporal perspective of Alaska tectonics is also needed for interpreting the MFFZ. Subduction has occurred in southern Alaska (or associated with the Wrangellia composite terrane) since at least 160 Ma and perhaps as early as 215 Ma, based on dated arc rocks, stratigraphic units, and plate reconstructions (Fisher and Magoon, 1978; Plafker and Berg, 1994; Rioux *et al.*, 2010). Notable perturbations include the subduction of a spreading ridge in southern Alaska at 61–50 Ma (Bradley *et al.*, 2003) and the collision and flat slab subduction of the Yakutat block starting by ~24 Ma and continuing today (Benowitz *et al.*, 2014). The stratigraphic record and seismically imaged subsurface structures in the Nenana basin provide a framework for understanding the local tectonic history (Fig. 5).

Transtensional Tectonic Setting

The modern-day, local tectonic setting of the MFFZ is transtensional, with the Nenana basin situated between two active left-lateral faults (Fig. 13). Stepovers in strike-slip faults are marked by a transtensional or transpressional setting, depending on the sense of the stepover, either releasing or restraining. A range of structures may occur in these settings, including pull-apart basins in transtensional settings (Mann *et al.*, 1983) or pop-up ridges in transpressional settings (Harland, 1971). Our study identifies two basin-bounding faults with left-lateral faulting between depths of 10 and 30 km, perhaps to the base of the crust.

The Dead Sea transform boundary between the Africa and Arabia plates is a well-studied transtensional setting (Garfunkel, 1981; ten Brink and Ben-Avraham, 1989; Ben-Avraham *et al.*, 2010) and provides a useful comparison for the MFFZ. The Dead Sea basin is a long, narrow, and deep sedimentary basin that forms at a fault stepover of the left-lateral Dead Sea transform. Katzman *et al.* (1995) presented 3D numerical models of crustal deformation in transtensional settings, using the Dead Sea basin as an example. They emphasized the importance of (1) the (fault-parallel) overlapping distance between the two left-lateral faults and (2) the (fault-normal) separation distance between the two faults (represented as shear zone width). Using an overlap of 50 km and a separation of 10 km, Katzman *et al.* (1995) produced a

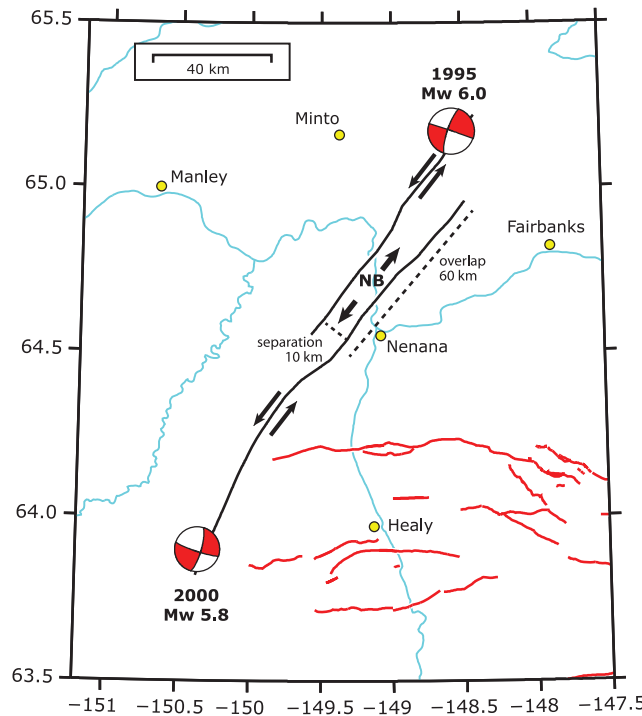


Figure 13. Active transtensional tectonic setting in the MFFZ. The two faults are digitized from seismicity, as shown in figure S4 of Tape *et al.* (2013); active faults are plotted in red (Koehler *et al.*, 2012). As plotted here, the western fault is 91 km in length, and the eastern fault is 159 km. The moment tensors in Figure 9 identify both faults as left lateral; they are separated by 10 km and overlap each other by 67 km. The current stage of the Nenana basin (labeled NB) is interpreted as a pull-apart basin between two left-lateral faults.

subsidence profile that was morphologically comparable to the Dead Sea basin. Additional 3D modeling efforts (numerical and analog) of pull-apart basins are presented in Gölke *et al.* (1994), Dooley and McClay (1997), and Petrunin and Sobolev (2008).

The transtensional setting in Minto Flats has some striking similarities with the Dead Sea region, as shown in Table 2. The Nenana basin has similar dimensions to the Dead Sea basin. Both basins are bounded to the west and east by faults, portions of which are seismically active, perhaps to the base of the crust. The ratio of fault separation to fault overlap—identified by Gölke *et al.* (1994) as a controlling parameter for basin formation—is 0.15 for Minto Flats and <0.20 for the Dead Sea. The seismic expression within the MFFZ (two seismic lineaments exhibiting left-lateral fault motion) appears to be simpler than that of the Dead Sea transform, where the seismic lineaments and style of faulting are not as clear (Aldersons *et al.*, 2003; Shamir, 2006; Braeuer *et al.*, 2014). The eastern boundary fault of the Dead Sea basin appears to be more active than the western boundary fault and is accommodating the left-lateral motion of the transform zone (Shamir, 2006).

It is possible that the Dead Sea and Nenana basins are influenced by vertical forces in the lower crust or upper man-

tle, in addition to the predominant lateral forces of transtension. Ten Brink *et al.* (2006) identified a low-velocity zone beneath the Dead Sea basin and hypothesized its origin from shear heating on the Dead Sea transform; the shear heating could in turn promote crustal flow and subsidence. Ben-Avraham and Schubert (2006) and Ben-Avraham *et al.* (2010) modeled Dead Sea basin formation and proposed that the deepest part has subsided because “an isolated block of lithosphere has dropped into the mantle,” possibly aided by high-density anomalies in the lower crust or upper mantle. Such hypotheses should be considered for the Nenana basin as well. It is possible that there are influences from the underlying mantle wedge, where Rondenay *et al.* (2010) imaged “strong coherent layering” and a globally exceptional 60 km discontinuity.

Early Tectonic History is Uncertain

There are two important differences between the Minto Flats and Dead Sea settings (Table 2): the total fault displacement and the slip rates. The Dead Sea transform has a well-documented slip rate of about 5 mm/yr, which is in agreement with geological slip rates inferred from a total displacement of 105 km over a period of ~20 Ma. The GPS displacement observations across the MFFZ exhibit large uncertainties, such that the slip rate would need to be a couple of millimeters per year to be distinguished (Fletcher, 2002; Freymueller *et al.*, 2008). In Table 2, we list 0–2 mm/yr based on the upper limit of 2 mm/yr assigned by Fletcher (2002) for the entire region, but it is likely that the actual slip rate is <0.5 mm/yr.

Based on published geological maps, there is little evidence for large-scale lateral displacements along the MFFZ. Newberry *et al.* (1996) mapped northeast-striking basement faults east of MFFZ and reported that “[a]pparent horizontal displacements of several kilometers to several meters are typical, and we infer vertical displacements of up to one kilometer” (p. 6). Along the northeastern trend of the MFFZ, there are no identifiable large offsets in bedrock units (Péwé *et al.*, 1966; Newberry *et al.*, 1996; Weber *et al.*, 1997); to the south, neither the seismic lineament of the MFFZ nor the Kantishna Hills anticline crosscut the Denali fault or is associated with lateral surface offsets (Fig. 2b).

The low active slip rate and presumably small long-term displacement in MFFZ mean we should probably not invoke a transtensional setting for the full >59 Ma history of the Nenana basin. We interpret the transtensional setting to be active for the past 6 Ma (Fig. 5). During this time period, the Nenana gravel was deposited (1.4 km in Nunivak-1) and thrusting began along the northern margin of the Alaska Range (Bemis *et al.*, 2015). Regionally the setting is north-south compression, consistent with left-lateral faulting on northeast-striking faults. Locally, the stepover in the MFFZ creates transtension, allowing the basin to subside.

The regional and local tectonic settings prior to 6 Ma are unclear. The Yakutat collision and Alaska Range uplift were

Table 2
Comparison between Dead Sea and Minto Flats Tectonic Settings

Parameter	Minto Flats	Reference*	Dead Sea	Reference*
Basin	Nenana basin	—	Dead Sea basin	—
Basin length	88 km	[D12]	132 km	T93
Basin width	12–15 km	[D12]	7–18 km	T93
Maximum basin depth	8.2 km	[D12]	10 km	T93
Maximum depth to Miocene sediments	2.5 km	V12	10 km	BS06
Youngest sediments in basin	Modern	—	Modern	T93
Fault system	Minto Flats fault zone	This study	Dead Sea transform	—
Length of fault system	180 km [†]	Figure 13	1000 km	BS06
Separation between basin-bounding faults	10 km	Figure 13	10 km	K95,[T93]
Overlap between basin-bounding faults	67 km	Figure 13	>50 km	K95,[T93],[S06]
Ratio of separation to overlap	0.15	—	<0.20	—
Depth range of sub-basin seismicity	7–24 km	Figure 6d	5–25 km	[S06]
Interplate or intraplate	Intraplate	—	Interplate	—
Strike-slip relative velocity	0–2 mm/yr	F02, F08	4.9 ± 1.4 mm/yr	L08
Total strike-slip displacement	Small/unknown		105 km	G81
Depth to Moho	25 km	WT14 (their fig. S3)	30 km	T06

*Square brackets are used when the number in the table is obtained based on information in the indicated study; in other cases, the number in the table is provided directly from the listed study. Code to references: BS06, Ben-Avraham and Schubert (2006); D12, Doyon Limited (2012); F02, Fletcher (2002); F08, Freymueller *et al.* (2008); G81, Garfunkel (1981); K95, Katzman *et al.* (1995); L08, Le Beon *et al.* (2008); S06, Shamir (2006); T06, ten Brink *et al.* (2006); T93, ten Brink *et al.* (1993); V12, Van Kooten *et al.* (2012); and WT14, Wang and Tape (2014).

[†]The 180 km length of the MFFZ, based on the digitized lines in Figure 13, is the sum of the overlapping sections (67 km), the nonoverlapping section of the west fault (91 km), and the nonoverlapping section of the east fault (22 km).

concurrent with the deposition of the Usibelli group, starting at ~24 Ma. Evidence of regional sedimentation (the Tanana basin of Ridgway *et al.*, 2007), uplift of the Alaska Range along the Denali fault (Benowitz *et al.*, 2011), and flat slab subduction provide support for a north–south (or northwest–southeast) compressional setting. (Authors such as Ridgway *et al.*, 2007, have used the term “transpressional” to imply the combined effects of large-scale strike-slip faulting, like Denali fault, with shortening caused by flat slab subduction. This use of the term is more generic than our use of “transtensional” as a basin forming along a stepover of a strike-slip fault [Katzman *et al.*, 1995]. To avoid confusion, we refer to the regional setting as compressional [Fig. 5], not transpressional.)

The local tectonic setting from 24 to 6 Ma appears to have been one of extension. Structural evidence within the Nenana basin indicates extension in the form of syntectonic filling of the half-graben (Van Kooten *et al.*, 2012). It is possible that the extensional structures in the basin are a manifestation of regional, not local, stresses. Rift basins (im-pactogens) can form at high angles to mountain belts (Şengör *et al.*, 1978; Şengör, 1995); a simplified perspective is that the principal compressional stress is perpendicular to the mountain belt, whereas the principal tensional stress is parallel to the mountain belt and perpendicular to the long axis of the rift basins. In this scenario, the Nenana basin and its basin-bounding faults would be aligned with the collisional direction and then undergo clockwise rotation into the present-day configuration.

It is possible that the local setting from 24 to 6 Ma was partly influenced by strike-slip faulting and was similar to the

setting today: regionally compressional but locally transtensional. It is possible that local, shallow extensional structures could form due to sub-basin strike-slip faulting at 15–25 km depths, such as the MFFZ today. There is significant uncertainty associated with strike-slip faulting in the MFFZ and similar faults to the east. Consider either the northeast-striking faults (Newberry *et al.*, 1996), which cut Paleozoic rocks, or the similarly trending seismic zones (Fig. S1). Much is unknown about these northeast-striking faults: when they formed, how they formed, their original strike direction, and their original sense of slip (i.e., dip slip or strike slip). Further geological and geophysical studies (Dixit and Hanks, 2014), as well as modeling efforts similar to those of Katzman *et al.* (1995), could help discriminate among different tectonic scenarios for the MFFZ and Nenana basin.

Possibility of Large ($M_w \geq 7$) Earthquakes

Field observations (Wesnousky, 1988, 2006; Lettis *et al.*, 2002) and numerical models (Harris *et al.*, 1991; Lozos *et al.*, 2012; Ryan and Oglesby, 2014) indicate that earthquakes can rupture through distinct fault segments within a fault zone. For example, the right-lateral strike-slip M_w 7.2 Landers, California, earthquake ruptured through five major fault segments (Sieh *et al.*, 1993; Madden *et al.*, 2013). Here, we first address the possibility of a fault rupture jumping between the two main faults of the MFFZ. We then consider the size of earthquakes that could be possible on each fault separately.

Wesnousky (2006) analyzed fault geometry and earthquake ruptures for 22 strike-slip earthquakes. He found that most ruptures terminate at fault endpoints or at fault steps that exceed 3–4 km. Lettis *et al.* (2002) found that earth-

quakes with larger displacements could propagate through fault stepovers with larger widths, up to 4–5 km. Rupture modeling indicates that ruptures are more likely to propagate through releasing bends (transtensional) than through restraining bends (transpressional) (Harris *et al.*, 1991; Ryan and Oglesby, 2014); however, observational evidence is equivocal (Wesnousky, 2006).

The stepover width, or fault separation, for the MFFZ is 10 km (Fig. 13). Therefore, we would not expect an earthquake rupture to jump between these faults, even given the theoretically favorable transtensional setting (versus transpressional). How large an earthquake is possible on each of the faults? The faults inferred from seismicity are approximately 90 km (west) and 160 km (east) in length (Fig. 13). We can estimate the magnitude of ruptures using the empirical scaling relationships of Mai and Beroza (2000) that are compiled from published finite-slip inversion models. For strike-slip faults, the scaling between moment and fault length is $\log_{10} L = 0.36 \log_{10} M_0 - 5.15$, in which L is in kilometers and M_0 is in newton-meters. To obtain an estimate for the mean slip on the fault, we use $M_0 = \mu A D$ and assume a rupture depth from 10 to 25 km and a crustal rigidity of $\mu = 35$ GPa. For a 20 km rupture length, we have $M_w 5.9$ and $D = 0.08$ m. For an 80 km rupture (west or east fault), we have $M_w 7.0$ and $D = 0.93$ m. For a 150 km rupture of the east fault, we have $M_w 7.5$ and $D = 2.84$ m. If we assume that the fault can rupture the entire length of the identified seismic lineament, then the west fault can produce an $M_w 7.0$ event and the east fault can produce an $M_w 7.5$ event. For comparison, Pulpan (1986) estimated a maximum magnitude of $M_s 7.0$ for the MFFZ, based on a fault length of 70 km.

We think that an $M_w 7.0$ – 7.5 earthquake within the MFFZ is possible. This estimate is based on the assumed fault length, which in turn is based on the continuity of seismicity and associated left-lateral slip. Earthquakes as large as $M_w 6.0$ have occurred in the fault zone (Fig. 11). The occurrence of an $M > 7$ earthquake in 1937 within the Salcha seismic zone, a similar left-lateral fault to the east, demonstrates that larger earthquakes are possible on the faults in this region. The 1937 earthquake was assigned a magnitude of $M 7.3$ by Gutenberg and Richter (1954) and was analyzed in Bramhall (1938), St. Amand (1948), and Fletcher and Christensen (1996).

The frequency–magnitude plots in Figure 6 imply recurrence intervals of centuries for large earthquakes. For example, within the MFFZ the recurrence intervals extrapolated from seismicity between $M_w 1.5$ – 3.5 are 105 years for $M_w \geq 6$, 770 years for $M_w \geq 7$, and 2100 years for $M_w \geq 7.5$. However, keep in mind that high-quality earthquake catalogs with small events have only existed for decades, not centuries: seismologists do not yet know how useful the frequency–magnitude distributions are for predicting recurrence for large earthquakes in any given region, as there are not enough data points. In some regions, it may be possible to estimate recurrence intervals using slip rates inferred from geodetic measurement or from moment tensor catalogs (Ward,

1998). The GPS velocity observations across the MFFZ are sparse, small, and have high uncertainties (Freymueller *et al.*, 2008). There is no GPS evidence for several millimeters per year left-lateral displacement rates across the MFFZ, suggesting that the longer recurrence rates could be appropriate. These long recurrence intervals combined with low slip rate and rapid sedimentation may act to obscure evidence of late Holocene ruptures on the floodplains of the Tanana and Nenana Rivers.

Conclusions

We present a seismological investigation of the MFFZ in central Alaska. Our key findings are as follows:

1. The MFFZ contains two primary faults, as delineated by seismicity. The MFFZ exhibits one of the largest concentrations of deep (≥ 15 km) crustal earthquakes in Alaska. Events on the western fault tend to be deeper than those on the eastern fault (median depths 17 km versus 14 km) (Fig. 6).
2. Moment tensor solutions from the best-recorded 11 events within the MFFZ reveal left-lateral faulting within all five subregions (Fig. 9). Among these events is the 29 November 2000 $M_w 5.7$ earthquake in the southern end of the MFFZ (Fig. 8).
3. The largest recorded earthquake in the MFFZ occurred at the northern end of the fault zone. The finite-slip model of the 1995 $M_w 6.0$ Minto Flats earthquake contains two slip patches within a rupture lasting 8 s (Fig. 11). The earthquake initiated with a slip patch that extended from depths of 9–19 km, with a peak slip of 57 cm. A second slip patch occurred shallower, between depths of 6 and 10 km, and to the north. The finite-slip model is consistent with left-lateral faulting on the western fault of the MFFZ.
4. The two main faults of the MFFZ overlap by 67 km and are separated by a 10 km stepover; between them is the 8-km-deep Nenana basin (Figs. 4 and 13). The occurrence of a narrow, deep, actively depositing basin between stepover faults in a strike-slip fault system is evidence for a transtensional tectonic setting. We compare the MFFZ tectonic setting with that of the well-studied Dead Sea region (Table 2).
5. Neither of the MFFZ faults has associated surface scarps or any other tectonic geomorphic features (Koehler *et al.*, 2012, 2015). Nevertheless, each fault coincides with a basin boundary (Fig. 4) and has continuity in microseismicity and style of faulting, leading us to propose the possibility of $M_w 7.0$ – 7.5 earthquakes. Based on frequency–magnitude distributions (Fig. 6), the recurrence interval for such earthquakes could be centuries, whereas the recurrence interval for an $M_w \geq 6.0$ event is approximately 100 years.
6. The potential occurrence of $M_w \geq 7$ earthquakes indicates that the MFFZ poses a seismic hazard to central Alaska

(particularly Fairbanks) and should be considered an active fault for the purposes of seismic-hazard assessments.

Tectonic models for central Alaska have regarded the MFFZ as the westernmost of a series of northeast-striking left-lateral faults (Page *et al.*, 1995; Bemis and Wallace, 2007; Haeussler, 2008; Bemis *et al.*, 2012, 2015). However, two features distinguish the MFFZ from neighboring left-lateral fault zones to the east. First, the MFFZ exhibits deeper earthquakes. Second, only the MFFZ has an associated deep sedimentary basin, as evidenced from gravity measurements (Figs. 3 and 4). The spatially larger, but shallow, Tanana basin to the east has been interpreted as a foreland basin influenced by the Alaska Range (Ridgway *et al.*, 2007); however, foreland influences can only partly account for the structure of the Nenana basin. The combination of the deep seismicity and the presence of a deep and active basin, together with modeling and observational inferences from the Dead Sea (Ben-Avraham *et al.*, 2010), raise the possibility that the Nenana basin is bounded by faults that extend to the base of the crust and enhance subsidence within this transtensional setting.

Our seismological study documents an active transtensional fault zone and basin. At the scale of Alaska, this 180-km-long fault zone is relatively small, and this transtensional setting is just one component of a broader intraplate deformation zone in central Alaska that exhibits larger-scale shear faulting (Page *et al.*, 1995), as well as thrusting to the south (Bemis and Wallace, 2007), all of which is driven by subduction and collision. Future geophysical efforts toward improving our understanding of the MFFZ and Nenana basin should come from (1) refinement of fault structures inferred from seismicity; (2) detailed passive and active seismic imaging of the basin, crust, and upper mantle; and (3) crustal deformation modeling that accounts for the transtensional setting (Katzman *et al.*, 1995) as well as the surrounding and underlying deformation zones.

Data and Resources

Seismic waveforms, including those from EarthScope's Transportable Array, were obtained from the Alaska Earthquake Center (AEC) and from the Incorporated Research Institutions for Seismology (IRIS) Data Management Center. The MATLAB Waveform Toolbox (Reyes and West, 2011) was used in processing the seismic waveforms, including the removal of the instrument response (MATLAB; www.mathworks.com/products/matlab; last accessed June 2015). Several figures were made using Generic Mapping Tools v.4.5.3 (Wessel and Smith, 1991). The digital data defining the basement surface in Figure 4 are proprietary and cannot be released to the public; however, they can be viewed at www.doyonoil.com (last accessed June 2015; Doyon Limited, 2012). The seismicity catalog for Alaska was obtained from the AEC and was last updated on 31 March 2015; for all analyses of seismicity, we exclude the events that were flagged as glacier events (G) or quarry blasts (Q).

Acknowledgments

We thank James Mery and Doyon Limited for providing their geophysical data, including the basement surface in Figure 4. Alicia Orange and Peggy Gallagher of Petrotechnical Resources of Alaska provided details on the geophysical data from Doyon. Amy McPherson supported our effort with ArcGIS expertise. Silvio DeAngelis created a custom waveform database for the 1995 M_w 6.0 Minto earthquake. This project was supported by National Science Foundation Grant EAR-1352668 (C. Tape) and by the Alaska Earthquake Center (V. Silwal). Our article benefitted from an anonymous review and an extensive review from Rich Koehler. We acknowledge helpful discussions with Wes Wallace, Jeff Benowitz, Nilesh Dixit, Jeff Freymueller, and Marwan Wartes, who also suggested considering Sengör (1995). We thank Tom Morahan for discussions on the structure of the Nenana basin.

References

- Ager, T. A., J. V. Matthews Jr., and W. Yeend (1994). Pliocene terrace gravels of the ancestral Yukon River near Circle, Alaska: Palynology, paleobotany, paleoenvironmental reconstruction and regional correlation, *Quaternary Int.* **22/23**, 185–206.
- Aldersons, F., Z. Ben-Avraham, A. Hofstetter, E. Kissling, and T. Al-Yazjeen (2003). Lower-crustal strength under the Dead Sea basin from local earthquake data and rheological modeling, *Earth Planet. Sci. Lett.* **214**, 129–142.
- Barnes, D. F. (1961). Gravity low at Minto Flats, in *Short Papers in the Geologic and Hydrologic Sciences, Articles 293–435*, Geological Survey Research 1961, U.S. Geol. Surv. Profess. Pap. 424-D, D254–D257.
- Beaudoin, B. C., G. S. Fuis, W. D. Mooney, W. J. Nokleberg, and N. I. Christensen (1992). Thin, low-velocity crust beneath the southern Yukon-Tanana terrane, east central Alaska: Results from Trans-Alaska Crustal Transect refraction/wide-angle reflection data, *J. Geophys. Res.* **97**, no. B2, 1921–1942.
- Bemis, S. P., and W. K. Wallace (2007). Neotectonic framework of the north-central Alaska Range foothills, in *Tectonic Growth of a Collisional Continental Margin: Crustal Evolution of Southern Alaska*, K. D. Ridgway, J. M. Trop, J. M. G. Glen, and J. M. O'Neill (Editors), Geol. Soc. Am., Boulder, Colorado, Special Paper 431, 549–572.
- Bemis, S. P., G. A. Carver, and R. D. Koehler (2012). The Quaternary thrust system of the northern Alaska Range, *Geosphere* **8**, no. 1, doi: 10.1130/GES00695.1.
- Bemis, S. P., R. J. Weldon, and G. A. Carver (2015). Slip partitioning along a continuously curved fault: Quaternary geologic controls on Denali fault system slip partitioning, growth of the Alaska Range, and the tectonics of south-central Alaska, *Lithosphere* **7**, 235–246, doi: 10.1130/L352.1.
- Ben-Avraham, Z., and G. Schubert (2006). Deep “drop down” basin in the southern Dead Sea, *Earth Planet. Sci. Lett.* **251**, 254–263.
- Ben-Avraham, Z., V. Lyakhovsky, and G. Schubert (2010). Drop-down formation of deep basins along the Dead Sea and other strike-slip fault systems, *Geophys. J. Int.* **181**, 185–197.
- Benowitz, J. A., P. W. Layer, P. Armstrong, S. E. Perry, P. J. Haeussler, P. G. Fitzgerald, and S. VanLaningham (2011). Spatial variations in focused exhumation along a continental-scale strike-slip fault: The Denali fault of the eastern Alaska Range, *Geosphere* **7**, 455–467.
- Benowitz, J. A., P. W. Layer, and S. VanLaningham (2014). Persistent long-term (*c.* 24 Ma) exhumation in the eastern Alaska Range constrained by stacked thermochronology, in *Advances in $^{40}\text{Ar}/^{39}\text{Ar}$ Dating: From*

- Archaeology to Planetary Sciences*, F. Jourdan, D. F. Mark, and C. Verati (Editors), Vol. 378, *Special Publications*, Geological Soc., London, doi: 10.1144/SP378.12.
- Biswas, N. N., and G. Tytgat (1988). Intraplate seismicity in Alaska, *Seismol. Res. Lett.* **59**, no. 4, 227–233.
- Bradley, D., T. Kusky, P. Haeussler, R. Goldfarb, M. Miller, J. Dumoulin, S. W. Nelson, and S. Karl (2003). Geologic signature of early Tertiary ridge subduction in Alaska, in *Geology of a Transpressional Orogen Developed during Ridge-Trench Interaction along the North Pacific Margin*, V. B. Sisson, S. M. Roeske, and T. L. Pavlis (Editors) *Geol. Soc. Am. Special Paper 371*, Boulder, Colorado, 19–49.
- Braeuer, B., G. Asch, R. Hofstetter, C. Haberland, D. Jaser, E. El-Kelani, and M. Weber (2014). Detailed seismicity analysis revealing the dynamics of the southern Dead Sea area, *J. Seismol.* **18**, 731–748.
- Bramhall, E. H. (1938). The central Alaska earthquake of July 22, 1937, *Bull. Seismol. Soc. Am.* **28**, 71–75.
- Cross, R. S., and J. T. Freymueller (2008). Evidence for and implications of a Bering plate based on geodetic measurements from the Aleutians and western Alaska, *J. Geophys. Res.* **113**, doi: 10.1029/2007JB005136.
- Dixit, N., and C. Hanks (2014). Tectono-thermal history of the southern Nenana basin, interior Alaska: Implications for conventional and unconventional hydrocarbon exploration, presented at *2014 Fall Meeting, AGU*, San Francisco, California, 15–19 December, Abstract T11A-4529.
- Dooley, T., and K. McClay (1997). Analog modeling of pull-apart basins, *Am. Assoc. Petro. Geol. Bull.* **81**, no. 11, 1804–1826.
- Doyon Limited (2012). *Nenana Basin Depth Map*, available at <http://doyonoil.com/HiResImage/NenDepthMap-ForWeb> (last accessed June 2015) (depth data and contours from Gary Thompson).
- Dziewonski, A., T.-A. Chou, and J. H. Woodhouse (1981). Determination of earthquake source parameters from waveform data for studies of global and regional seismicity, *J. Geophys. Res.* **86**, no. B4, 2825–2852.
- Ehm, A. (1983). Oil and gas basins map of Alaska, *Alaska Div. Geol. Geophys. Surv. Spec. Rept. 32*.
- Ekström, G., M. Nettles, and A. M. Dziewoński (2012). The Global GCMT project 2004–2010: Centroid-moment tensors for 13,017 earthquakes, *Phys. Earth Planet. In.* **200/201**, 1–9.
- Ferris, A., G. A. Abers, D. H. Christensen, and E. Veenstra (2003). High resolution image of the subducted Pacific (?) plate beneath central Alaska, 50–150 km depth, *Earth Planet. Sci. Lett.* **214**, 575–588.
- Finzel, E. S., L. M. Flesch, and K. D. Ridgway (2011). Kinematics of a diffuse North America-Pacific–Bering plate boundary in Alaska and western Canada, *Geology* **39**, no. 9, 835–838.
- Fisher, M. A., and L. B. Magno (1978). Geologic framework of lower Cook Inlet, *Am. Assoc. Petro. Geol. Bull.* **62**, no. 3, 373–402.
- Fletcher, H. (2002). Crustal deformation in Alaska measured using the Global Positioning System, *Ph.D. thesis*, University of Alaska Fairbanks, Alaska.
- Fletcher, H. J., and D. H. Christensen (1996). A determination of source properties of large intraplate earthquakes in Alaska, *Pure Appl. Geophys.* **146**, no. 1, 21–41.
- Freymueller, J. T., H. Woodard, S. C. Cohen, R. Cross, J. Elliott, C. F. Larsen, S. Hreinsdóttir, and C. Zweck (2008). Active deformation processes in Alaska, based on 15 years of GPS measurements, in *Active Tectonics and Seismic Potential of Alaska*, J. T. Freymueller, P. J. Haeussler, R. Wesson, and G. Ekström (Editors), American Geophysical Union Monograph 179, 1–42.
- Frohman, R. A. (2014). Identification and evolution of tectonic faults in the greater Fairbanks area, Alaska, *Master's Thesis*, University of Alaska Fairbanks, Alaska.
- Fuis, G. S., T. E. Moore, G. Plafker, T. M. Brocher, M. A. Fisher, W. D. Mooney, W. J. Nokleberg, R. A. Page, B. C. Beaudoin, N. I. Christensen *et al.* (2008). Trans-Alaska crustal transect and continental evolution involving subduction underplating and synchronous foreland thrusting, *Geology* **36**, no. 3, 267–270.
- Garfunkel, Z. (1981). Internal structure of the Dead Sea leaky transform (rift) in relation to plate kinematics, *Tectonophysics* **80**, 81–108.
- Gedney, L., S. Estes, and N. Biswas (1980). Earthquake migration in the Fairbanks, Alaska seismic zone, *Bull. Seismol. Soc. Am.* **70**, no. 1, 223–241.
- Gedney, L., L. Shapiro, and D. VanWormer (1972). Correlation of epicenters with mapped faults, east-central Alaska, 1968–1971, *U.S. Geol. Surv. Open-File Rept. 72-128*, 7 pp., 1 map.
- Gölke, M., S. Cloetingh, and K. Fuchs (1994). Finite-element modeling of pull-apart basin formation, *Tectonophysics* **240**, 45–57.
- Gutenberg, B., and C. F. Richter (1954). *Seismicity of the Earth and Associated Phenomena*, Second Ed., Princeton University Press, Princeton, New Jersey.
- Haeussler, P. J. (2008). An overview of the neotectonics of interior Alaska: Far-field deformation from the Yakutat microplate collision, in *Active Tectonics and Seismic Potential of Alaska*, J. T. Freymueller, P. J. Haeussler, R. Wesson, and G. Ekström (Editors), American Geophysical Union Monograph 179, 83–108.
- Haeussler, P. J., D. C. Bradley, R. E. Wells, and M. L. Miller (2003). Life and death of the Resurrection plate: Evidence for its existence and subduction in the northeastern Pacific in Paleocene–Eocene time, *Geol. Soc. Am. Bull.* **115**, no. 7, 867–880.
- Haeussler, P. J., A. Matmon, D. P. Schwartz, and G. Seitz (2014). The Denali fault slip rate and models of interior Alaska active deformation, presented at the *2014 SSA Annual Meeting*, Anchorage, Alaska, 30 April–2 May 2014.
- Harland, W. B. (1971). Tectonic transpression in Caledonian Spitsbergen, *Geol. Mag.* **108**, 27–42.
- Harris, R. A., R. J. Archuleta, and S. M. Day (1991). Fault steps and the dynamic rupture process: 2-D numerical simulations of a spontaneously propagating shear fracture, *Geophys. Res. Lett.* **18**, no. 5, 893–896.
- Hawthorne, J. C., and J.-P. Ampuero (2013). Using phase coherence to search for and examine foreshock activity, in *2013 Southern California Earthquake Center Annual Meeting, Proceedings and Abstracts*, Palm Springs, California, 8–11 September 2013, Vol. 23, 235 pp.
- Huang, P. Y., and N. N. Biswas (1983). Rampart seismic zone of central Alaska, *Bull. Seismol. Soc. Am.* **73**, no. 3, 813–829.
- Ji, C., D. V. Helmberger, D. J. Wald, and K.-F. Ma (2003). Slip history and dynamic implications of the 1999 Chi-Chi, Taiwan, earthquake, *J. Geophys. Res.* **108**, no. B9, doi: 10.1029/2002JB001764.
- Ji, C., D. J. Wald, and D. V. Helmberger (2002). Source description of the 1999 Hector Mine earthquake; Part I: Wavelet domain inversion theory and resolution analysis, *Bull. Seismol. Soc. Am.* **92**, 1207–1226.
- Katzman, F., U. S. ten Brink, and K. Lin (1995). Three-dimensional modeling of pull-apart basins: Implications for the tectonics of the Dead Sea basin, *J. Geophys. Res.* **100**, no. B4, 6295–6312.
- Koehler, R. D., R.-E. Farrell, P. A. C. Burns, and R. A. Combierick (2012). Quaternary faults and folds in Alaska: A digital database, *Alaska Div. Geol. Geophys. Surv. Miscellaneous Publication 141*, 31 pp, 1 sheet, scale 1:3,700,000.
- Koehler, R. D., R. D. Reger, E. R. Spangler, and A. I. Gould (2015). Investigation of potentially active tectonic faults along the route of the proposed Alaska Stand Alone Pipeline, Livengood to Cook Inlet, Alaska, *Alaska Div. Geol. Geophys. Surv. Report of Investigations 2015-4*, 78 pp.
- Koons, P. O., B. P. Hooks, T. Pavlis, P. Upton, and A. D. Barker (2010). Three-dimensional mechanics of Yakutat convergence in the southern Alaskan plate corner, *Tectonics* **29**, doi: 10.1029/2009TC002463.
- Langston, C. A., and D. V. Helmberger (1975). A procedure for modelling shallow dislocation sources, *Geophys. J. Roy. Astron. Soc.* **42**, 117–130.
- Le Beon, M., Y. Klinger, A. Q. Amrat, A. Agnon, L. Dorbath, G. Baer, J.-C. Ruegg, O. Charade, and O. Mayyas (2008). Slip rate and locking depth from GPS profiles across the southern Dead Sea Transform, *J. Geophys. Res.* **113**, doi: 10.1029/2007JB005280.
- Leonard, L. J., S. Mazzotti, and R. D. Hyndman (2008). Deformation rates estimated from earthquakes in the northern Cordillera of Canada and eastern Alaska, *J. Geophys. Res.* **113**, doi: 10.1029/2007JB005456.

- Leopold, E. B., and G. Lu (1994). A long pollen sequence of Neogene age, Alaska Range, *Quaternary Int.* **22/23**, 103–140.
- Lesh, M. E., and K. D. Ridgway (2007). Geomorphic evidence of active transpressional deformation in the Tanana foreland basin, south-central Alaska, in *Tectonic Growth of a Collisional Continental Margin: Crustal Evolution of Southern Alaska*, K. D. Ridgway, J. M. Trop, J. M. G. Glen, and J. M. O'Neill (Editors), *Geol. Soc. Am. Special Paper 431*, Boulder, Colorado, 573–592.
- Lettis, W., J. Bachhuber, R. Witter, C. Brankman, C. E. Randolph, A. Barka, W. D. Page, and A. Kaya (2002). Influence of releasing step-overs on surface fault rupture and fault segmentation: Examples from the 17 August 1999 Izmit earthquake on the North Anatolian fault, Turkey, *Bull. Seismol. Soc. Am.* **92**, no. 1, 19–42.
- Lozos, J. C., D. D. Oglesby, J. N. Brune, and K. B. Olsen (2012). Small intermediate fault segments can either aid or hinder rupture propagation at stepovers, *Geophys. Res. Lett.* **39**, doi: 10.1029/2012GL053005.
- Mackey, K. G., K. Fujita, L. V. Gunbina, V. N. Kovalev, V. S. Imaev, B. M. Koz'min, and L. P. Imaeva (1997). Seismicity of the Bering Strait region: Evidence for a Bering block, *Geology* **25**, no. 11, 979–982.
- Madden, E. H., F. Maerten, and D. D. Pollard (2013). Mechanics of non-planar faults at extensional steps with application to the 1992 $M = 7.3$ Landers, California, earthquake, *J. Geophys. Res.* **118**, 3249–3263, doi: 10.1002/jgrb.50237.
- Mai, P. M., and G. C. Beroza (2000). Source scaling properties from finite-fault-rupture models, *Bull. Seismol. Soc. Am.* **90**, no. 3, 604–615.
- Mann, P., M. R. Hempton, D. C. Bradley, and K. Burke (1983). Development of pull-apart basins, *J. Geol.* **91**, 529–554.
- Marshak, R. S., and D. E. Karig (1977). Triple junctions as a cause for anomalously near-trench igneous activity between the trench and volcanic arc, *Geology* **5**, no. 4, 233–236.
- Mazzotti, S., and R. D. Hyndman (2002). Yakutat collision and strain transfer across the northern Canadian Cordillera, *Geology* **30**, no. 6, 495–498.
- Miller, M. L., D. C. Bradley, T. K. Bundtzen, and W. McClelland (2002). Late Cretaceous through Cenozoic strike-slip tectonics of southwestern Alaska, *J. Geol.* **110**, no. 3, 247–270, doi: 10.1086/339531.
- Newberry, R. J., T. K. Bundtzen, K. H. Clautice, R. A. Combellick, T. Douglas, G. M. Laird, S. A. Liss, D. S. Pinney, R. R. Reifenstuhl, and D. N. Solie (1996). Preliminary geologic map of the Fairbanks Mining District, Alaska, *Alaska Div. Geol. Geophys. Surv. Public Data File 96-16*, 17 pp., 1 sheet, scale 1:63,360.
- Page, R. A., G. Plafker, and H. Pulpan (1995). Block rotation in east-central Alaska: A framework for evaluating earthquake potential? *Geology* **23**, no. 7, 629–632.
- Petrunin, A. G., and S. V. Sobolev (2008). Three-dimensional numerical models of the evolution of pull-apart basins, *Phys. Earth Planet. In.* **171**, 387–399.
- Pewé, T. L., C. Wahrhaftig, and F. R. Weber (1966). Geologic map of the Fairbanks Quadrangle, *U.S. Geol. Survey Miscellaneous Investigation Series I-455*.
- Plafker, G., and H. C. Berg (1994). Overview of the geology and tectonic evolution of Alaska, in *Geology of Alaska*, G. Plafker and H. C. Berg (Editors), *The Geology of North America*, Vol. G-1, Chapter 33, Geol. Soc. Am., Boulder, Colorado, 989–1021.
- Pulpan, H. (1986). Seismic-hazard analysis of the Nenana Agricultural Development Area, central Alaska, *Alaska Div. Geol. Geophys. Surv. Public-Data File 86-78*.
- Ratchkovski, N. A., and R. A. Hansen (2002). New constraints on tectonics of interior Alaska: Earthquake locations, source mechanisms, and stress regime, *Bull. Seismol. Soc. Am.* **92**, no. 3, 998–1014.
- Redfield, T. F., D. W. Scholl, P. G. Fitzgerald, and M. E. Beck Jr. (1997). Escape tectonics and the extrusion of Alaska: Past, present, and future, *Geology* **35**, no. 11, 1039–1042.
- Reyes, C. G., and M. E. West (2011). The Waveform Suite: A robust platform for manipulating waveforms in MATLAB, *Seismol. Res. Lett.* **82**, 104–110.
- Ridgway, K. D., E. E. Thoms, P. W. Layer, M. E. Lesh, J. M. White, and S. V. Smith (2007). Neogene transpressional foreland basin development on the north side of the central Alaska Range, Usibelli group and Nenana gravel, Tanana basin, in *Tectonic Growth of a Collisional Continental Margin: Crustal Evolution of Southern Alaska*, K. D. Ridgway, J. M. Trop, J. M. G. Glen, and J. M. O'Neill (Editors), 507–547, *Geol. Soc. Am. Special Paper 431*, Boulder, Colorado.
- Ridgway, K. D., J. M. Trop, and A. R. Sweet (1997). Thrust-top basin formation along a suture zone, Cantwell basin, Alaska Range: Implications for development of the Denali fault system, *Geol. Soc. Am. Bull.* **109**, no. 5, 505–523.
- Rioux, M., J. Mattinson, B. Hacker, P. Kelemen, J. Blusztajn, K. Hanghøj, and G. Gehrels (2010). Intermediate to felsic middle crust in the accreted Talkeetna arc, the Alaska Peninsula and Kodiak Island, Alaska: An analogue for low-velocity middle crust in modern arcs, *Tectonics* **29**, doi: 10.1029/2009TC002541.
- Rondenay, S., L. G. J. Montési, and G. A. Abers (2010). New geophysical insight into the origin of the Denali volcanic gap, *Geophys. J. Int.* **182**, 613–630.
- Ruppert, N. A. (2008). Stress map for Alaska from earthquake focal mechanisms, in *Active Tectonics and Seismic Potential of Alaska*, J. T. Freymueller, P. J. Haeussler, R. Wesson, and G. Ekström (Editors), American Geophysical Union Monograph 179, 351–367.
- Ruppert, N. A., K. D. Ridgway, J. T. Freymueller, R. S. Cross, and R. A. Hansen (2008). Active tectonics of interior Alaska: Seismicity, GPS, and local geomorphology, in *Active Tectonics and Seismic Potential of Alaska*, J. T. Freymueller, P. J. Haeussler, R. Wesson, and G. Ekström (Editors), American Geophysical Union Monograph 179, 109–133.
- Ryan, K. J., and D. D. Oglesby (2014). Dynamically modeling fault step overs using various friction laws, *J. Geophys. Res.* **119**, 5814–5829, doi: 10.1002/2014JB011151.
- Saltus, R. W., P. J. Brown II, R. L. Morin, and P. L. Hill (2008). 2006 compilation of Alaska gravity data and historical reports, *U.S. Geol. Survey Digital Series 264*, CD-ROM.
- Sengör, A. M. C. (1995). Sedimentation and tectonics of fossil rifts, in *Tectonics of Sedimentary Basins*, C. J. Busby and R. V. Ingersoll (Editors), Chapter 2, Blackwell, Oxford, London, 53–117.
- Sengör, A. M. C., K. Burke, and J. F. Dewey (1978). Rifts at high angles to orogenic belts: Tests for their origin and the Upper Rhine graben as an example, *Am. J. Sci.* **278**, 24–40.
- Shamir, G. (2006). The active structure of the Dead Sea Depression, in *New Frontiers in Dead Sea Paleoenvironmental Research*, Y. Enzel, A. Agnon, and M. Stein (Editors), *Geol. Soc. Am. Special Paper 401*, Boulder, Colorado, 15–32.
- Shao, G., X. Li, C. Ji, and T. Maeda (2011). Focal mechanism and slip history of the 2011 M_w 9.1 Off the Pacific Coast of Tohoku earthquake, constrained with teleseismic body and surface waves, *Earth Planets Space* **63**, 559–564, doi: 10.5047/eps.2011.06.028.
- Sieh, K., L. Jones, E. Hauksson, K. Hudnut, D. Eberhart-Phillips, T. Heaton, S. Hough, K. Hutton, H. Kanamori, A. Lilje, et al. (1993). Near-field investigations of the Landers earthquake sequence, April to July 1992, *Science* **260**, 171–176.
- St. Amand, P. (1948). The central Alaska earthquake swarm of October 1947, *Eos Trans. AGU* **29**, no. 5, 613–623.
- Tape, C., M. West, V. Silwal, and N. Ruppert (2013). Earthquake nucleation and triggering on an optimally oriented fault, *Earth Planet. Sci. Lett.* **363**, 231–241.
- Tape, W., and C. Tape (2012). A geometric setting for moment tensors, *Geophys. J. Int.* **190**, 476–498.
- ten Brink, U. S., and Z. Ben-Avraham (1989). The anatomy of a pull-apart basin: Seismic reflection observations of the Dead Sea basin, *Tectonics* **8**, no. 2, 333–350.
- ten Brink, U. S., A. S. Al-Zoubi, C. H. Flores, Y. Rotstein, I. Qabbani, S. H. Harder, and G. R. Keller (2006). Seismic imaging of deep low-velocity zone beneath the Dead Sea basin and transform fault: Implications for strain localization and crustal rigidity, *Geophys. Res. Lett.* **33**, doi: 10.1029/2006GL027890.
- ten Brink, U. S., Z. Ben-Avraham, R. E. Bell, M. Hassouneh, D. F. Coleman, G. Andreasen, G. Tibor, and B. Coakley (1993). Structure of the Dead

- Sea pull-apart basin from gravity analyses, *J. Geophys. Res.* **98**, no. B12, 21,877–21,894.
- Triplehorn, D. M., J. Drake, and P. W. Layer (2000). Preliminary Ar³⁹/Ar⁴⁰ ages from two units in the Usibelli group, Healy, Alaska: New light on some old problems, in *Short Notes on Alaska Geology 1999*, D. S. Pinney and P. K. Davis (Editors), *Alaska Div. Geol. Geophys. Surv. Professional Report 119*, 117–127.
- Van Kooten, G. K., M. Richter, and P. A. Zippi (2012). Alaska's Interior rift basins: A new frontier for discovery, *Oil Gas J.* **110**, no. 1a, 48–57.
- Veenstra, E., D. H. Christensen, G. A. Abers, and A. Ferris (2006). Crustal thickness variation in south-central Alaska, *Geology* **34**, no. 9, 781–784.
- Wahrhaftig, C., J. A. Wolfe, E. B. Leopold, and M. A. Lanphere (1969). The Coal-Bearing group in the Nenana Coal Field, Alaska, *U.S. Geol. Surv. Bull. 1274-D*, Contributions to Stratigraphy series.
- Waldhauser, F., and W. L. Ellsworth (2000). A double-difference earthquake location algorithm: Method and application to the northern Hayward fault, California, *Bull. Seismol. Soc. Am.* **90**, no. 6, 1353–1368.
- Wang, Y., and C. Tape (2014). Seismic velocity structure and anisotropy of the Alaska subduction zone derived from surface wave tomography, *J. Geophys. Res.* **119**, 8845–8865, doi: 10.1002/2014JB011438.
- Ward, S. N. (1998). On the consistency of earthquake moment rates, geological fault data, and space geodetic strain: The United States, *Geophys. J. Int.* **134**, 172–186.
- Wartes, M. W., R. J. Gillis, T. M. Herriott, R. G. Stanley, K. P. Helmold, C. S. Peterson, and J. A. Benowitz (2013). Summary of 2012 reconnaissance field studies related to the petroleum geology of the Nenana basin, interior Alaska, *Alaska Div. Geol. Geophys. Surv. Preliminary Interpretive Report 2013–2*, 13 pp.
- Weber, F. R., K. L. Wheeler, C. D. Rinehart, and T. D. Light (1997). Generalized geologic map of the Livengood Quadrangle, Alaska, U.S. Geol. Surv. Open-File Rept. 97-484-A, 1 sheet, scale 1:250,000.
- Wesnousky, S. G. (1988). Seismological and structural evolution of strike-slip fault, *Nature* **335**, 340–343.
- Wesnousky, S. G. (2006). Predicting the endpoints of earthquake ruptures, *Nature* **444**, 358–360.
- Wessel, P., and W. H. F. Smith (1991). Free software helps map and display data, *Eos Trans. AGU* **72**, no. 41, 441–446.
- Zhu, L., and D. Helmberger (1996). Advancement in source estimation techniques using broadband regional seismograms, *Bull. Seismol. Soc. Am.* **86**, no. 5, 1634–1641.
- Geophysical Institute
University of Alaska
903 Koyukuk Drive
Fairbanks, Alaska 99775
ctape@alaska.edu
(C.T., V.S., L.K., M.E.W., N.R.)
- Department of Earth Science
University of California
Webb Hall 2036
Santa Barbara, California 93106
(C.J.)

Manuscript received 18 February 2015;
Published Online 21 July 2015